# Statistical Physics of glassy systems: tools and applications

Pierfrancesco Urbani[1,*]

[1] *Institut de physique théorique, Université Paris Saclay, CNRS, CEA, F-91191 Gif-sur-Yvette*

January 17, 2018

These are the notes of the lectures I gave at the Institut de Physique Théorique during November-December 2017. All the material contained here is not original and we make always reference to original papers. This is a draft version.



*Electronic address: pierfrancesco.urbani@ipht.fr

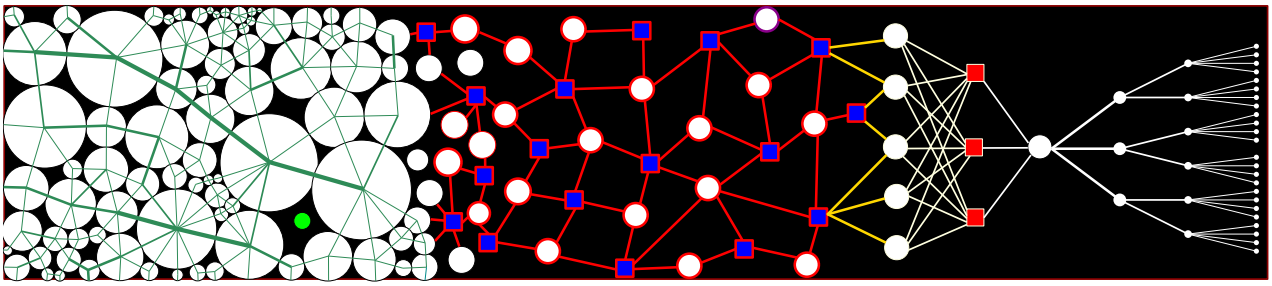

**Contents**

## I. INTRODUCTION

The complex behavior of a large variety of systems can be often ascribed to the competition of many quasi-optimal equilibria. In these cases metastability deeply affects both the structural and dynamical properties. Glasses are the prototype of such systems, with glassy behavior arising not only in condensed matter but also in a wide variety of fields ranging from optimization to computer science.

In these lectures I will introduce different kinds of glassy systems and I will describe their fundamental similarities, which emerge from their statistical description. Then I will focus on a representative model, the random perceptron, and I will discuss the main techniques that can be used to solve it.

These techniques provide a versatile theoretical toolbox that can be applied to several problems such as for example the physics of the jamming transition, its interpretation in the context of constraint satisfaction, as well as the design of new efficient algorithms to solve statistical problems.

The plan of these lectures is the following. In the first section I will discuss the similarities between basically two classes of glassy systems: structural glasses and constraint satisfaction problems. I will first describe qualitatively what are glasses and how they form. In order to do that I will focus on the simplest structural glass model given by hard spheres. Then I will introduce one of the theories that aim at explaining the glass transition and I will discuss that it becomes exact in the limit of infinite dimension. I will describe a set of phase diagrams and physical observables that can be used to characterize the glass transition. Then I will discuss a prototypical constraint satisfaction problem, the random coloring problem and I will show what is its phase diagram underlying the similarities and differences with hard spheres. Finally I will introduce a simplified model, the random perceptron, as a tradeoff between hard spheres and constraint satisfaction problems.

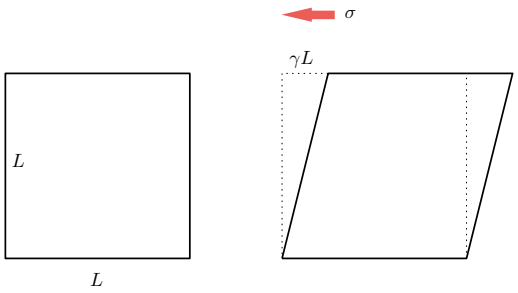


FIG. 1: The deformation of a solid of linear size $L$. $\gamma$ is defined as the amount of deformation induced by the stress $\sigma$.

The remaining section are devoted to the study of the random perceptron as a paradigm of glassy systems.

## II. WHAT IS A GLASS

Glasses are special kinds of solids that do not posses crystalline order. What defines a solid is its way of responding to external perturbations. Indeed, unlike for liquids, in order to deform a solid one needs to apply a force (see fig. (1)).

However at the microscopic length scale glasses are disordered structures. Indeed looking at how the atoms or molecules are organized in space one can distinguish two classes of solids[1]:

- *crystalline solids*: the elementary degrees of freedom (atoms or molecules) are organized in a regular lattice. This can be usually studied using group theory and the physics of crystals can be understood in terms of perturbations or deformations of this underlying regular structure.
- *amorphous solids*: the elementary degrees of freedom are positioned at random in space in the sense that there is no evident underlying order that can be seen from a snapshot of the microscopic configurations. In particular two typical configurations of the same system, one in the liquid phase and another one in the amorphous solid phase, look practically indistinguishable.

It is clear that in crystalline solids symmetry is crucial and many properties of the system can be obtained from that. Instead, amorphous solids are intrinsically disordered and it is not clear which is the right way to describe them.

### A. Basic phenomenology of the glass transition

In order to understand the physics of amorphous solids we briefly describe how they form using a simple glass former: *hard spheres*.

[1] Here we will not speak about quasi-crystals. The interested reader can look at [1].

We take a system of $N$ hard spheres of diameter $D$ in $d$ dimensions in a volume $V$ [2, 3]. The hard sphere pairwise potential is zero unless the spheres overlap. In the latter case it is infinity thus prohibiting spheres to overlap. Since the spheres must be non overlapping, one can consider the fraction of space occupied by them that is called the packing fraction. If $\rho = N/V$ is the density of spheres and $\mathcal{V}_d(D)$ is the volume of a sphere with diameter $D$, the packing fraction is $\varphi = \rho\mathcal{V}_d$. The packing fraction is a control parameter and by changing it one can drive the system towards different phase transitions as we will show below.

Let us consider the dynamics of a gas of hard spheres starting from an intial configuration at low packing fraction. In this case it is very easy to find a configuration of non overlapping spheres. Starting from that, we can initialize their velocities extracting them from a Maxwell distribution at a given temperature $T$. Note that because of the hard sphere potential, in this case the temperature is irrelevant and it gives only a time scale for particle collisions. In other words, there is only kinetic energy since the potential energy is always zero.[2]

Given the velocities we can run the Newton's equation of motion. According to this, particles move at constant velocity unless they collide. The result of an elastic collision can be computed from momentum and energy conservation [4]. This dynamical algorithm is called *molecular dynamics* and it really simulates the real dynamics of a hard sphere gas.

Starting from a low density configuration, we can consider what happens upon compression. This can be obtained either by reducing the volume accessible to the system or by increasing the diameter of the particles. In both cases one can introduce a compression rate $\gamma$ that is the rate at which either the volume accessible to the system is reduced or the radius of the spheres is increased. The evolution of the system depends crucially on the compression rate.



### 1. *Adiabatic compression and crystallization*

Let us first consider what happens for $\gamma \to 0$ in $d = 3$. In this case the system is compressed adiabatically and therefore one expects that it will follow the *equilibrium equation of state*. In order to describe it one can introduce the pressure. This is given in terms of the momentum transferred by the particles colliding with the walls in which the system is contained. Since the pressure is clearly proportional to the temperature (being $T$ just a timescale for collisions) one usually defines a *reduced* pressure as $p(\varphi) = P\beta/\rho$ where $P$ is the actual pressure and $\beta = 1/T$.

Starting from a small packing fraction, the pressure increases up to when the system undergoes a first order transition toward a crystalline state organized around a face centered cubic (FCC) lattice. This happens at the freezing packing fraction $\varphi_f$ where the system jumps to a crystalline state with a packing fraction $\varphi_m$.

In the crystalline state, on a first approximation, the spheres just vibrate around the nodes of the crystalline lattice. Upon compression, the amplitude of vibrations is reduced up to a point where the system jams into a perfect FCC crystalline lattice packing. At this point the reduced pressure diverges: the system cannot be compressed further because the spheres cannot overlap.

This is what happens for $\gamma \to 0$ in sufficiently low dimensions ($d = 2,\ 3$). In higher dimensions, the situation is expected to be similar but we know the densest lattice packings only in few other examples ($d = 8,\ 24$) [5, 6]. In particular it is not clear if in the $d \to \infty$ limit there is a crystallization transition and what is the density of

---

[2] Hard Spheres are models for colloidal suspensions or granular materials. For these systems temperature is irrelevant because the interaction potential is very singular. However for more general systems like molecular glasses, for which the interaction potential between the degrees of freedom is a smooth function, temperature plays a central role and is an additional control parameter. We call these systems *thermal* glasses.

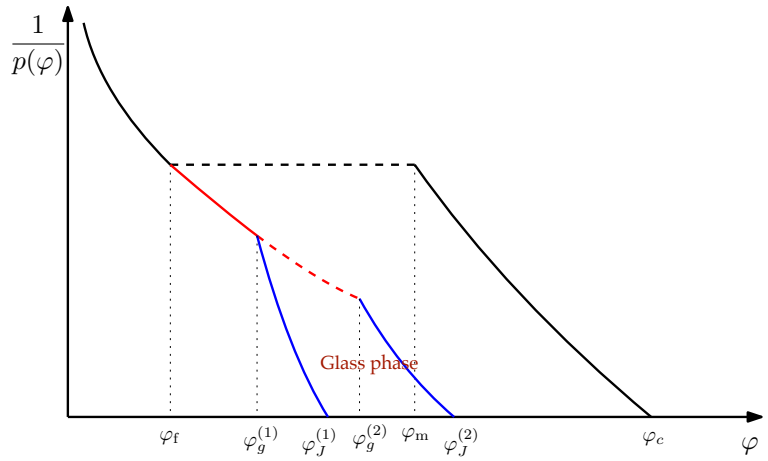


FIG. 2: The phenomenological phase diagram of hard spheres under compression (a sketchy reproduction of the one contained in [2].). $\varphi_{\rm f}$ and $\varphi_{\rm m}$ are respectively the freezing and melting packing fraction of the crystalline state. $\varphi_{\rm c}$ is the packing fraction of the corresponding crystalline jammed structure. $\varphi_g^{(1)} \equiv \varphi_g(\gamma_1)$ is the glass transition point of the system when compressed with compression rate $\gamma_1$. $\varphi_J^{(1)}$ is the jamming packing fraction of the glass in which the system has fallen at $\varphi_g^{(1)}$. $\varphi_g^{(2)}$ and $\varphi_J^{(2)}$ are the same quantities obtained for $\gamma_2 < \gamma_1$.



the densest packing [7–9]. In Fig. (2) we represent the equilibrium equation of state with a solid black curve.

### 2. *Finite compression rate and vitrification*

The situation changes when the compression rate $\gamma$ is kept finite. In this case, for sufficiently fast compression rates[3] one can avoid the crystallization transition and the system enters in a metastable phase that is called *supercooled* [4]. This is represented by the solid red curve in Fig. (2).

Along the compression protocol one can measure the relaxation time of the system in the following way. One can define the dynamical Mean Square Displacement (MSD) as

$$\Delta(t) = \frac{1}{N}\sum_{i=1}^{N} |x_i(t) - x_i(0)|^2 \,. \tag{1}$$

Here $x_i(t)$ is the position of particle $i$ at a given time $t$. The MSD is a measure of similarity between the configuration at time zero and the one reached at time $t$; it is equal to zero if the two configurations are the same.

---

[3] Here we do not enter into the details of how fast should be the compression rate [2, 10]. This in fact depends on the nucleation process of the underlying crystal and depends strongly on the dimension. In particular, going to higher dimension decreases the minimal compression rate needed to avoid crystallization since, heuristically, the crystalline structure becomes more difficult to find due to the dimensionality bottleneck.

[4] This terminology comes from thermal glasses where the system comes from a high temperature liquid phase and enters in a metastable supercooled phase when it is cooled sufficiently fast thus avoiding the crystallization transition.

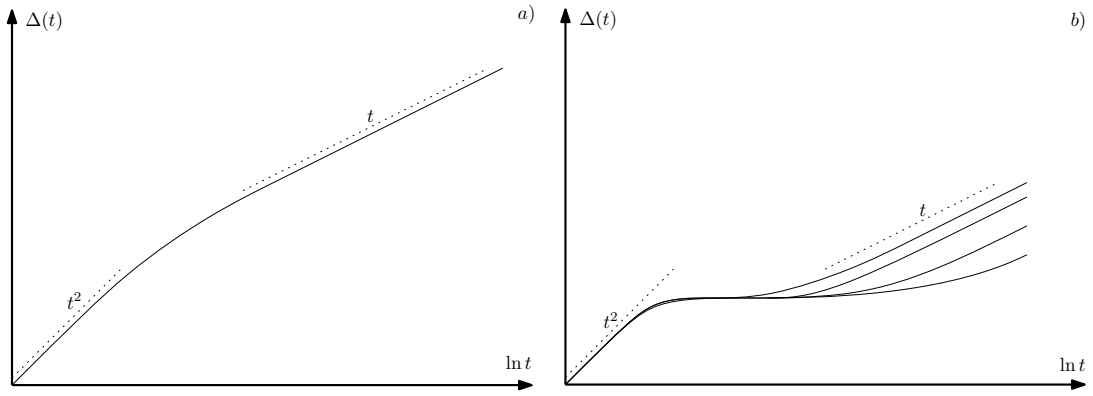


FIG. 3: The behavior of the MSD at different packing fractions. (a) At low packing fractions the MSD has a first ballistic increase and the a diffusive one. (b) Deep in the supercooled region the ballistic and diffusive regime are separated by a plateau whose length increases exponentially when the packing fraction increases.

At sufficiently low density in the supercooled phase the shape of the MSD is the one reported in Fig. 3.a. For short times it has a ballistic regime where $\Delta(t) \sim t^2$. This is due to the fact that if the time window $t$ is sufficiently small, particles move freely since they did not have time to collide. The ballistic regime is followed by a diffusive one where the the motion of particles is deeply affected by collisions. In this regime $\Delta(t) \sim t$. The relaxation time $\tau_\alpha$ can be seen roughly as how long it takes for the system to reach the diffusive regime.

Upon compression, in the supercooled phase the MSD starts to develop a plateau as depicted in Fig. (3.b) Deep in the supercooled regime, the relaxation time increases of several orders of magnitude upon compression. Typically, this increase is so large that a possible fit of the behavior of $\tau_\alpha$ when changing the packing fraction would be $\tau_\alpha \sim \exp\left(A/|\phi - \phi^*|^\delta\right)$ for some constants $\phi^*$, $A$ and $\delta$ [11]. Practically, at a packing fraction $\varphi_g$ the relaxation time becomes so large that the system does not relax on *simulation* time scales. This is the glass transition point. The system is frozen into an amorphous solid, an hard sphere glass, and is not able to relax to the metastable supercooled liquid phase.

The glass transition point $\varphi_g$ depends on the compression rate $\gamma$. For $\gamma_1 < \gamma_2$ one has $\varphi_g(\gamma_1) > \varphi_g(\gamma_2)$. In Fig. (2) we display two glass transition points for two different compression rates.

Once the system is frozen into a glass, when further compressed, its equation of state leaves the one of the supercooled liquid. In Fig. (2) we show the equation of state of two different glasses prepared with two different compression rates. Upon compression, at $\widehat{\varphi}_J(\gamma)$ these hard sphere glasses undergo a jamming transition where the pressure diverges since the spheres get in touch forming a rigid network of contacts.

Jammed packings of hard spheres have been shown to share universal features [2, 3, 12–16]. First of all one can focus on the network of contacts between spheres. It can be shown that the average connectivity $z$ of this network is $z = 2d$. This property is called *isostaticity* and ensures the mechanical stability of the packings. Furthermore one can properly define a network of forces between spheres that are in contact. It can be shown that the distribution of contact forces $P(f)$ follows a power law behavior

$$P(f) \sim f^\theta \qquad f \to 0\,. \tag{2}$$

In an analogous way one can measure the statistics of gaps between spheres that are not in contact. The gap between two spheres of diameter $D$ at positions $x_i$ and $x_j$ is defined as

$$h_{ij} = |x_i - x_j| - D \tag{3}$$

and it is found that the distribution of gaps has a power law behavior

$$g(h) \sim h^{-\gamma_J} \qquad h \to 0^+ \,. \tag{4}$$

As we will discuss in the following sections, these critical exponents reflect the fact that amorphous jammed packings are *marginally stable*.

#### 3. *The glass transition problem*

The glass transition problem can be summarized as follows: what are the mechanisms that drive the freezing of the supercooled liquid into the glass? As we have said, the glass phase is apparently as much amorphous or disordered as the supercooled liquid one, and therefore no simple symmetry breaking line of reasoning can be employed to understand this phenomenon. Many theories have been proposed to tackle this problem [17, 18]. Instead of reviewing them in these notes I will rather focus on a particular one that is called the *Random first order transition theory* [19–22]. The reason for this is that the scenario emerging from this theory is realized in the limit in which the dimension is sent to infinity and structural glass models can be exactly solved.

According to this picture, sufficiently deep in the supercooled region the phase space gets clustered in a large number of metastable states, that are what we call glasses. In finite dimensions these amorphous structures have a finite, albeit very long, lifetime. Deep in the supercooled liquid phase, the dynamical relaxation can be thought as a set of jumps from one metastable state to another. These jumps are well separated in time and between them the system relaxes inside the metastable states exploring them in an ergodic fashion. Compressing (or cooling) the system the lifetime of metastable visited increase in an exponential way eventually diverging at thermodynamic transition known as the Kauzmann transition point [23].

In infinite dimension these glassy states have infinite lifetime and therefore can be studied using static tools [10, 24].



### B. The infinite dimensional solution of the hard sphere model

The theory of amorphous states of hard spheres can be *exaclty* solved in the infinite dimensional limit [25–30]. Although I will not describe it I will present the emerging phase diagram that can be obtained. This is represented in Fig. (4). On the $x$-axis there is the *scaled* packing fraction that is defined as $\widehat{\varphi} = 2^d \varphi / d$ and on the $y$-axis there is the inverse of the *scaled reduced pressure* $\widehat{p} = p/d$. The red line is again the equilibrium supercooled liquid line. Note that there is no first order phase transition to any crystal. This is due to the fact that in large dimensions we do not know the crystal structure and therefore we do not know where the crystal appears.

Upon compression the dynamical MSD develops a two step relaxation as in Fig. (3.b) [31]. However in this case the relaxation time $\tau_\alpha$ diverges with a power law at a well defined scaled packing fraction $\widehat{\varphi}_{\rm d}$ as $\tau_\alpha \sim |\widehat{\varphi} - \widehat{\varphi}_{\rm d}|^{-\gamma_{\rm MCT}}$ with an exponent $\gamma_{\rm MCT}$ that can be computed analytically [26]. At $\widehat{\varphi}_{\rm d}$ the system develops an extremely large number of glassy states. If the initial condition for the dynamical evolution is a typical configuration of one of such glassy states, the system will stay trapped there forever[5]. In particular the long

[5] This statement can be made precise. If we take *first* the thermodynamic limit $N \to \infty$ and then we take the long time limit, the system will never escape from the glass state. Instead if we take first the long time limit and only *after* the $N \to \infty$ limit, the system will be able to escape from the state.

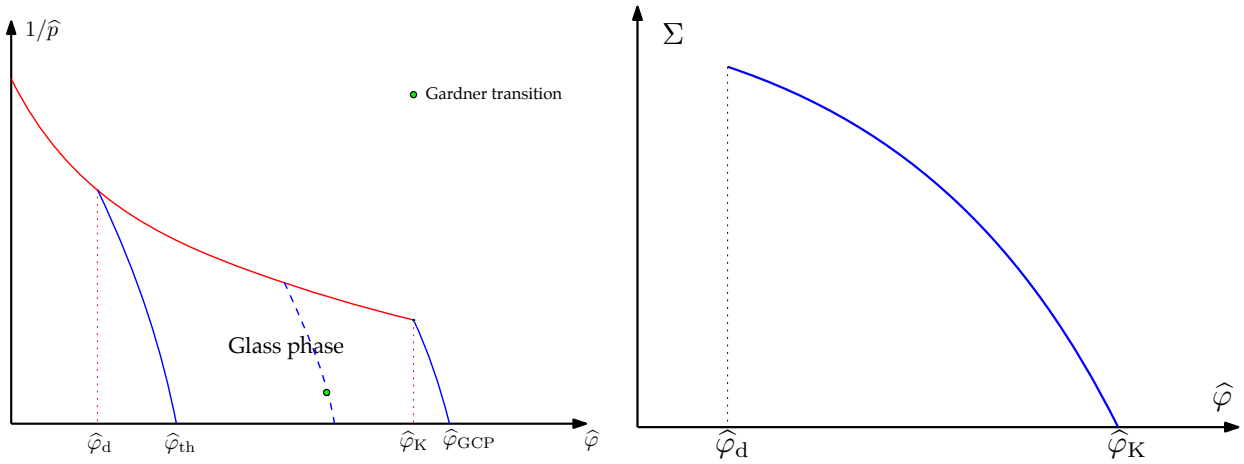


FIG. 4: a) The phase diagram of hard spheres in infinite dimension (from [3, 27, 28]). $\widehat{\varphi}_{\rm d}$, $\widehat{\varphi}_K$ and $\widehat{\varphi}_{\rm GCP}$ are respectively the dynamical, Kauzmann and Glass close packing transition point. The red line is the equation of state of the supercooled liquid. The dashed line is the equation of state of a given glass of hard spheres upon compression. b) The configurational entropy as a function of the packing fraction (from [2, 3]).

time limit of the MSD is finite

$$\lim_{t\to\infty} \Delta(t) = \Delta_{\rm EA} < \infty \,. \tag{5}$$

This means that the spheres are blocked inside local cages formed by the surrounding ones and vibrate inside this amorphous structure. This is summarized in Fig. (5). The phase transition that happens at $\widehat{\varphi}_{\rm d}$ is an ergodicity breaking point. It is called *dynamical* transition in the context of spin glasses and *Mode-Coupling transition* in the context of structural glasses [32].

In order to understand better what happens at $\widehat{\varphi}_{\rm d}$ one can look at the phase space accessible to the dynamics. In the supercooled phase, particles can diffuse and can explore the whole phase space and therefore the dynamics is ergodic. At $\widehat{\varphi}_{\rm d}$ the phase space gets clustered into an exponential number of glassy states. These are portions of phase space that are mutually inaccessible one from the other. If the initial configuration of the dynamics is inside one of these states, the system will never reach configurations that are typical of other glassy states. From the thermodynamic point of view nothing happens at $\widehat{\varphi}_{\rm d}$. The free energy is analytic and therefore there is no thermodynamical phase transition.

The number of glassy states that appear at $\widehat{\varphi}_{\rm d}$ is exponential in the system size and therefore one can associate an entropy to them [33]. This is given by

$$\Sigma = \lim_{N\to\infty} \frac{1}{N} \ln \mathcal{N} \tag{6}$$

being $\mathcal{N}$ the number of glassy states. The quantity $\Sigma$ is called *configurational entropy*. Its shape as a function of the scaled packing fraction is shown in Fig. (4.b). It is maximal at $\widehat{\varphi}_{\rm d}$ and decreases upon increasing the packing fraction.

When $\widehat{\varphi} \to \widehat{\varphi}_{\rm K}$ the configurational entropy vanishes. This is called the Kauzmann transition point. For $d \to \infty$ one has that $\widehat{\varphi}_{\rm K} \sim \ln d$. Unlike for the dynamical transition, the Kauzmann point is a true thermodynamic phase transition that is of the *Random First order type* [18].

Compressing adiabatically the system beyond the Kauzmann transition point, the system leaves the supercooled equation of state and remains frozen into an *ideal glass* state. Compressing further, the ideal glass jams

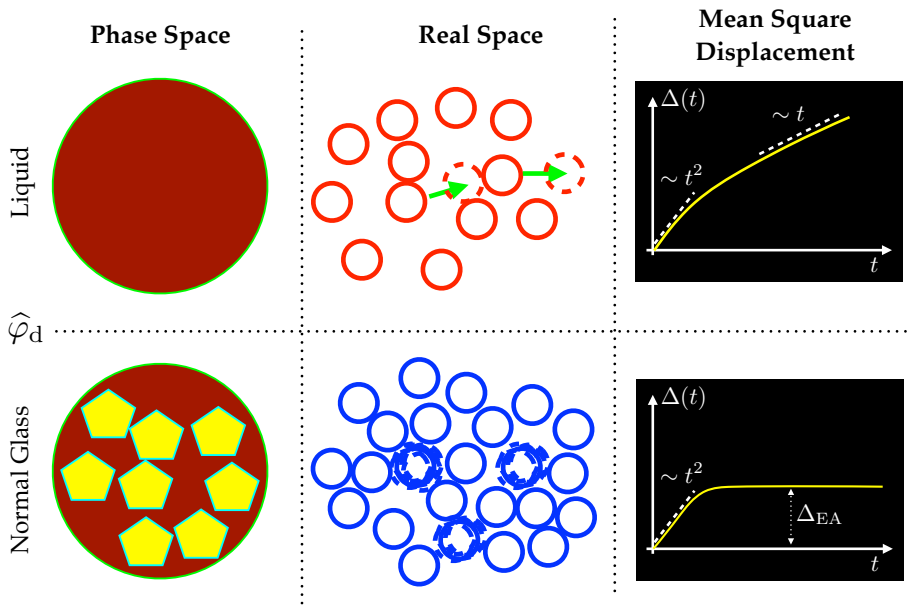


FIG. 5: The mean field dynamical transition for hard spheres seen in terms of phase space, mean square displacement and real space. (From [3])



at the so called *Glass Close Packing* point. This represent the densest amorphous structure. Note that since $\widehat{\varphi}_{\rm K} \sim \ln d$, $\widehat{\varphi}_{\rm GCP} \sim \ln d$ too.

If we neglect the eventual crystalline jammed packing that can be formed, $\widehat{\varphi}_{\rm GCP}$ represent a *satisfiability transition point*. For $\widehat{\varphi} > \widehat{\varphi}_{\rm GCP}$ no amorphous packing of non overlapping spheres can be found. We underline here that the satisfiability threshold is in the glass phase.

Instead of looking at what happens below the Kauzmann transition point one could see what happens to glass states when they are compressed. If we assume that our compression rate is finite, the system will not be able to escape from the glass state and the evolution will leave the equilibrium supercooled liquid line. This is the dashed line represented in Fig. 4a. What happens upon compression is that at some point there is a new phase transition that is called the Gardner transition where the system enters in a so called *marginally stable* phase. We will see what this means in the following. Then, compressing further, the system will jam. The properties of amorphous jammed packings in large dimensions can be also computed exactly and one can show first that theyare isostatic at jamming, and, second, that they are critical. The computation of the critical exponents of the force and gap distributions can be also done and we will review it in a simplified model for jamming. However we stress here that the jamming transition *within* a glass state can be seen as a satisfiability threshold transition *within that state*.

### C. The glassy phase of constraint satisfaction problems

We want now to discuss another class of glassy systems, namely constraint satisfaction problems [34]. A constraint satisfaction problem (CSP) can be defined in the following way [35].

Consider a set of $N$ variables $X = \{x_i\}$, with $i = 1, \dots, N$, taking values in a given set $\mathcal{S}$, and a set of $M$ constraints, labelled by the index $\alpha = 1, \dots M$. Each constraint $\alpha$ involves a certain number of variables $k_\alpha$ that we call $X_\alpha = \{x_1^{(\alpha)}, \dots, x_{k_\alpha}^{(\alpha)}\}$. Furthermore we call $k_\alpha$ the *connectivity* of the constraint $\alpha$ and $\mathcal{S}_\alpha$ the set of all possible values that can be taken by $X_\alpha$. A constraint $\alpha$ can be defined as a binary function

$$\psi_\alpha : \mathcal{S}_\alpha \to \{0, 1\} . \tag{7}$$

We say that if $\psi_\alpha(X_\alpha) = 1$ the constraint $\alpha$ is satisfied by the assignment $X_\alpha$ otherwise $\psi_\alpha(X_\alpha) = 0$.

Therefore a general constraint satisfaction problem can be summarized in finding a configuration (or the set of configurations) that satisfy the following global constraint

$$1 = \prod_{\alpha=1}^{M} \psi_\alpha(X_\alpha) . \tag{8}$$

The network of variables entering in the constraints can be visualized in a so called *factor graph*. This is represented in Fig. (6) where each circle represents a variable while each square denotes a constraint. The variables are connected to the constraints in which they enter.

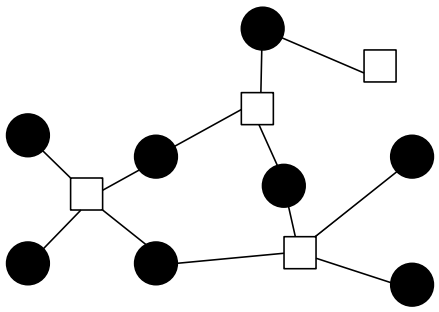

FIG. 6: A factor graph. The circles represent variables, while the squares denote the constraints.



An instance of a CSP can be specified by giving:

- The set $\mathcal{S}$ in which the variables $X$ take values;
- The nature of the constraints;
- The factor graph: this specifies all the connectivities $k_\alpha$ and the sets $X_\alpha$.

Given a CSP one can ask different questions. For example [35]:

- **Decision**: understand whether a CSP admits solutions or not;
- **Sampling**: if the CSP admits solutions, find one;
- **Optimization**: Finding the minimal number of violated constraints.

In particular one would like to know how many solutions a given CSP has. This is given by

$$Z = \sum_{X} \prod_{\alpha=1}^{M} \psi_\alpha(X_\alpha) . \tag{9}$$

### 1. Random constraint satisfaction problems

In computational complexity theory [36], CSPs can be classified according to their difficulty. However it is clear that the notion of the difficulty of a CSP strictly depends on the particular instance of the problem. For example one can imagine to formulate a CSP with zero constraints. This trivially admits as many solutions as the volume of $\mathcal{S}$. Therefore the notion of computational complexity strictly relies on some particular instance of a given CSP.

In computer science one is typically interested in the so called *worst case*: given a CSP one wants to understand how difficult is the most difficult instance taken from a given set of CSPs.

However one can imagine to define a probability measure on the instances of a given class of CSPs. For example one can throw at random the factor graph. In this case it is clear that one could be more interested in the *typical case*.

These *random* CSPs can be treated with means of statistical physics. In particular, if the probability measure over the instances of the CSPs has some particular features, one can use tools from spin glasses to compute the phase diagram of random CSPs [34, 37–42]. Here we will not review how CSPs can be solved in the most general case. For the moment we will limit ourselves to describe the phase diagram emerging from a given CSP, the random coloring problem, and we will argue that this is very close to hard spheres. Then we will introduce a particular CSP, the random perceptron and we will solve it using different techniques.

### 2. Discrete variables: the random coloring problem

The random coloring problem can be defined as follows. Each variable $x_i = \{1, \dots, q\}$ can take only $q$ possible values, the colors. Moreover, in this case a constraint $\alpha$ depends only on two variables and therefore $k_\alpha = 2$ for all $\alpha$. Denoting with $x_1^{(\alpha)}$ and $x_2^{(2)}$ the two variables entering in the constraint $\alpha$, this can be written as

$$\psi_\alpha(X_\alpha) \equiv \psi_\alpha(x_1^{(\alpha)}, x_2^{(\alpha)}) = 1 - \delta_{x_1^{(\alpha)}, x_2^{(\alpha)}} \tag{10}$$

which means that the two variables entering in $\alpha$ must have different colors. Given the variables and the nature of the constraints we have to characterize the factor graph in order to completely specify the CSP. There are two classes of factor graphs that can be solved analytically:

- **Erdös-Renyi random graphs**: each of the $M$ constraints $\alpha$ is defined by extracting at random with a flat measure a couple of variables from the $\binom{N}{2}$ possible distinct couples. It can be shown that when $N, M \to \infty$ with $M/N = \tilde{\alpha}$, the connectivity of each variable $c$ is a random variable with Poisson distribution of average $\overline{c} = 2\tilde{\alpha}$.

- **Regular random graphs**: each variable enters in exactly $c$ constraints and therefore the connectivity of the variable nodes of the factor graph is fixed. A factor graph is extracted with a uniform measure over all the factor graphs that satisfy this property. In this case we have that $2M = cN$ and therefore $\tilde{\alpha} = c/2$.

Once an ensemble of factor graphs is chosen, the random coloring problem becomes well defined. The phase diagram of this CSP depends only on two independent control parameters that are the number of colors $q$ and the connectivity $c$. Having fixed the number of colors, one can ask if a typical CSP with at a given connectivity $c$ is satisfiable (SAT) or not (UNSAT), which means if that problem admits an assignment of $X$ that satisfies all the constraints. One can expect that for small values of $c$, there are very few constraints and a typical instance is SAT. Conversely, increasing the connectivity, it becomes harder to find a SAT assignment. Given a factor graph $\mathcal{G}$ with average connectivity $c_\mathcal{G}$ one can ask for the probability that a SAT assignment exists. Let us

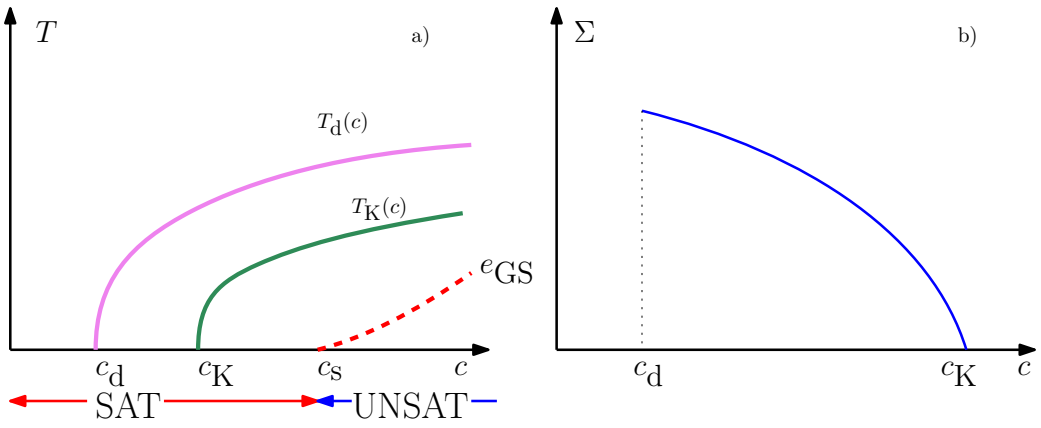


FIG. 7: a) The phase diagram of the coloring problem. $T_{\rm d}(c)$ is the dynamical transition line where the Monte Carlo algorithm fails to equilibrate. At $T_{\rm K}(c)$ there is a static transition where the complexity of glassy states goes to zero. This is the Kauzmann transition point and the equilibrium measure has a phase transition. These pictures are sketches taken from [44].

call this probability $\mathbf{P}$. It turns out that for $N \to \infty$, the probability $\mathbf{P}$ is a function of $c$. Moreover there is a precise point, that is called the satisfiability threshold $c_s$ such that

$$\mathbf{P}(c) = \begin{cases} 1 & c < c_s \\ 0 & c > c_s \, . \end{cases} \tag{11}$$

In order to understand how the space of solutions of the random coloring looks like in the SAT region, for $c < c_s$ one can imagine to design an algorithm to find them. In order to do so, we can recast this problem in a statistical physics setting.

We define an energy function that depends on the configuration $X$ of the variable nodes of the factor graph. The energy is defined as follows:

$$E(X) = \sum_{\alpha=1}^{M} (1 - \psi_\alpha(X_\alpha)) = \sum_{\alpha=1}^{M} \delta_{x_i^{(\alpha)}, x_j^{(\alpha)}} \equiv \sum_{\langle i,j \rangle} \delta_{x_i, x_j} \tag{12}$$

where the sum over $\langle i, j \rangle$ runs over all couples that enter in the constraints. This energy function just counts the number of unsatisfied constraints. It is clear that it is nothing else than the energy function of an antiferromagnetic Potts model [43] defined on a random graph. A SAT assignment of the CSP is equivalent to a zero energy configuration of the corresponding Potts model and therefore is a zero energy ground state.

In order to find the ground state one can imagine to set up a *simulated annealing* algorithm. From now on we will consider a random coloring problem with $q \geq 4$ [6]. We introduce a temperature $T$ and we run a Monte Carlo (MC) dynamics starting from $T = \infty$. Then we start to cool the system slightly changing the temperature ideally with an infinitesimal cooling rate. It turns out that only if $T > T_{\rm d}(c)$ the Monte Carlo algorithm is able to equilibrate. Instead below $T_{\rm d}(c)$ the dynamics gets stuck. In the connectivity *vs* temperature phase diagram, one can trace a line $T_{\rm d}(c)$ where this happens and this is plotted in Fig. 7.

The zero temperature limit of this phase diagram tells us what happens to the space of solutions of the random coloring problem.

[6] For $q < 4$ the phase diagram is different and we will not discuss it here.

For $c < c_{\rm d}$ the space of solutions form a unique cluster. This means that if we start from a solution of the model, then *local search algorithms* are able to explore the whole space of solutions. Their dynamics is exploring ergodically all the solutions.

At $c_{\rm d}$ instead the space of solutions splits into a large number of clusters. Therefore $c_{\rm d}$ is called a *clustering* transition and it is analogous to the dynamical transition that we have described for hard spheres in infinite dimensions. If a local search algorithm is initialized in a solution that belongs to a cluster it will explore all the other solutions belonging to it but it will not be able to jump to the other clusters. Therefore each cluster has a finite *internal entropy* and is disconnected from the others. The internal entropy of a cluster can be defined as the logarithm of the number of solutions present in that cluster.

The number of clusters of solutions is exponential in the system size. In an analogous way to glasses one can define the number of clusters as a function of $c$. This is represented in Fig. (7.b). In this context this quantity is called the complexity. When $c \to c_{\rm K}$ the complexity of the relevant clusters of solutions (the ones with largest entropy) go to zero. This is a Kauzmann transition point of the same kind of the one happening in the infinite dimensional solution of structural glass models. In the context of random CSPs, the Kauzmann transition is typically called a *condensation* transition.

Increasing the connectivity, at $c_{\rm s}$ all clusters of solutions disappear. This is the SAT/UNSAT threshold where in the thermodynamic limit no solution can be found. From the antiferromagnetic Potts model point of view, at $c_{\rm s}$ the ground state energy becomes positive, since there is a finite fraction of violated constraints.

In the coloring problem there is an additional phase transition, compared to the hard sphere case, that is called the *rigidity transition*. This happens only at zero temperature and it is the point where there are frozen variables in the dominant clusters of solutions. Frozen variables are variables nodes that are fixed to the same value in all solutions belonging to a given cluster. The rigidity transition $c_{\rm r}$ appears for $c_{\rm r} > c_{\rm d}$ but can happen both before or after the condensation transition $c_{\rm K}$.



### 3. *Summary: from hard spheres to CSPs and back: fundamental similarities and differences*

In the previous sections we have presented two phase diagrams: on the one hand we have shown how the infinite dimensional solution of the hard sphere model capture some essential features of the glass formation. On the other we have discussed the phase transitions in a random CSP, the random coloring.

The striking observation is that the phase diagrams of both models are remarkably similar in the sense that the phase transitions that can be driven changing the packing fraction or the connectivity are of the same nature.

We can make a list of similar points:

- In both models at the dynamical or clustering transition point the phase space accessible to the microscopic degrees of freedom splits into an exponential number of clusters or basins of configurations that are called glassy states.
- Any local dynamics started from a typical configuration inside one of these states will remain trapped there.
- The number of glassy states, being locally stable amorphous solids as in spheres, or clusters of solution in the random coloring, scale exponentially with the system size.
- At the Kauzmann or condensation transition, the configurational entropy or complexity vanishes and the a true thermodynamic phase transition takes place.

- Both the hard sphere model and the random coloring problem display a satisfiability transition point. This phase transition happens deep in the glass phase and therefore in order to understand its properties one needs to fully characterize the statistics of glass basins.

The first three points of this list are quite generic in the sense that they appear in the mean field treatment of many glassy systems. Actually one would have the tendency to say that they could be regarded as the hallmarks of glassiness at the mean field theory level. Instead the last point pertains only to contexts where a satisfiability transition takes place. This phase transition is well defined only at zero temperature and for models where the interaction energy has finite range. Indeed it is clear that it is not possible to strictly define a satisfiability transition point for a model of Lennard-Jones particles.

Furthermore, under the light of CSPs, one can think about hard spheres as a CSP. Indeed in the hard sphere problem one needs to find configurations of phases space in which the spheres do not overlap. In this way, the molecular dynamics that we have discussed above can be roughly thought as a local search algorithm. Starting from a SAT assignment for the positions of the spheres, the MD is exploring other SAT assignments by making local movements and therefore it has a clear algorithmic interpretation.

Despite these fundamental similarities, there are however also some differences. First of all, the hard sphere model has no quenched disorder while the random coloring does since the factor graph is taken randomly from a specified ensemble. Nevertheless the phase transitions remain the same.

Furthermore, the hard sphere model is a CSP for *continuous* variables which are the positions of the spheres. Instead in the coloring problem variables can take values in a discrete set. This has an important consequence. At the SAT/UNSAT threshold of the coloring problem the entropy of the relevant clusters of solutions stays finite at the transition. Instead in the hard sphere models, the entropy of the hard sphere glasses goes to minus infinity because the system shrinks to one configuration. Furthermore it is clear that having continuous variables allow the system to develop scaling behavior close to jamming while this does not happen at the SAT/UNSAT transition point for discrete CSP [45, 46]. The scaling and universal behavior indeed can be described using a set of power laws that we will obtain in the following sections.

In order to fill the gap between random discrete CSPs and hard sphere glasses we will introduce a model that has features coming both from hard spheres and random CSP. This model is the *spherical random perceptron* [45, 46]. In this section we introduce it and we give the main properties of the model.

The rest of these lectures is devoted to solve this model with different methods coming from statistical physics.



### *4. The spherical random perceptron*

Let us consider a CSP with $N$ variables $x_i$ with $i = 1, \dots, N$ and $x_i \in \mathbb{R}$. These variables are subjected to a *global* spherical constraint that enforces the condition

$$\sum_{i=1}^{N} x_i^2 = N \tag{13}$$

and therefore each variable is of order 1. We will indicate with $\underline{X} = \{x_1, \dots, x_N\}$ the global state of the $N$ variables.

Next we introduce a set of $M$ *patterns* $\underline{\xi}^\mu$ with $\mu = 1, \dots, M$. Each pattern is an $N$-dimensional vector whose components are denoted as $\underline{\xi}^\mu = \{\xi_1^\mu, \dots, \xi_N^\mu\}$. The components of each vector $\underline{\xi}^\mu$ are independent identically distributed Gaussian random variables with zero mean and unit variance. Furthermore the number of patterns is $M = \alpha N$ being $\alpha$ a constant of order one that will play a role of a control parameter of the model.

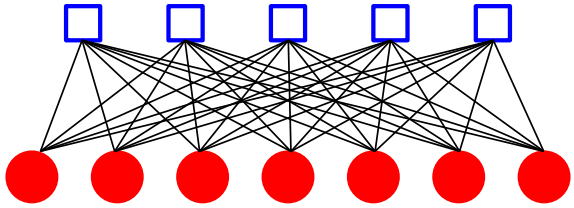

FIG. 8: The factor graph of the perceptron mode for $M = 5$ and $N = 7$.

Next we define a *gap* variable. For each pattern $\xi^\mu$ we introduce

$$h_\mu = \frac{1}{\sqrt{N}} \underline{\xi}^\mu \cdot \underline{X} - \sigma \tag{14}$$

where $\sigma$ is the second control parameter of the model. Note that since both $\xi_i^\mu$ and $x_i$ are of order one, the scalar product $\underline{\xi}^\mu \cdot X$ is of order $\sqrt{N}$ by central limit theorem and therefore, globally, gap variables are of order one.

Given the set of gap variables, one can define a constraint satisfaction problem by asking to find a configuration of $X$ that satisfy the following constraints:

$$h_\mu > 0 \qquad \forall \mu = 1, \dots, M. \tag{15}$$

In an analogous way with respect to the coloring problem, we can define an energy cost function given by

$$H[X] = \frac{1}{2} \sum_{\mu=1}^{M} h_\mu^2 \theta(-h_\mu) \tag{16}$$

Therefore, for every violated constraint, the energy cost is proportional to the square of the corresponding gap variable. The factor graph corresponding to this CSP is described in Fig. 8.

**Analogy with soft spheres.** - The energy const function of Eq. (16) is constructed in analogy with soft spheres. In this case the spheres have a finite range interaction; if $r_i$ and $r_j$ are the positions of two spheres, their interaction potential is

$$V_{ij} = \frac{1}{2} \left( |r_i - r_j| - D \right)^2 \theta \left[ D - |r_i - r_j| \right] \tag{17}$$

where $D$ is the diameter of the spheres. Therefore the parameter $\sigma$ plays the same role as the diameter and the gap variable $h_\mu$ is analogous to the gab between the spheres $h_{ij}$.

**The geometry of phase space and convexity.** - The geometry of phase space can be easily visualized. Let us consider one pattern $\underline{\xi}^\mu$. The constraint is such that

$$\underline{\xi}^\mu \cdot \underline{X} > \sqrt{N} \sigma \, . \tag{18}$$

There are two possibilities depending on the sign of the control parameter $\sigma$. Let us consider $\sigma > 0$. In Fig. 9.a we plot a two dimensional projection of the $N$ dimensional sphere. The red arc denotes the allowed region of phase space while the blue arc denote the forbidden region. Therefore in this case the allowed region of phase space is *convex*.

In Fig. 9.b instead we plot what happens for $\sigma < 0$. In this case the allowed region of phase space is *non convex*.

In order to solve the CSP we need to find a configuration $\underline{X}$ that satisfies all constraints. For $\sigma > 0$, the allowed region of phase space is the intersection of convex domains on the sphere. The intersection of convex

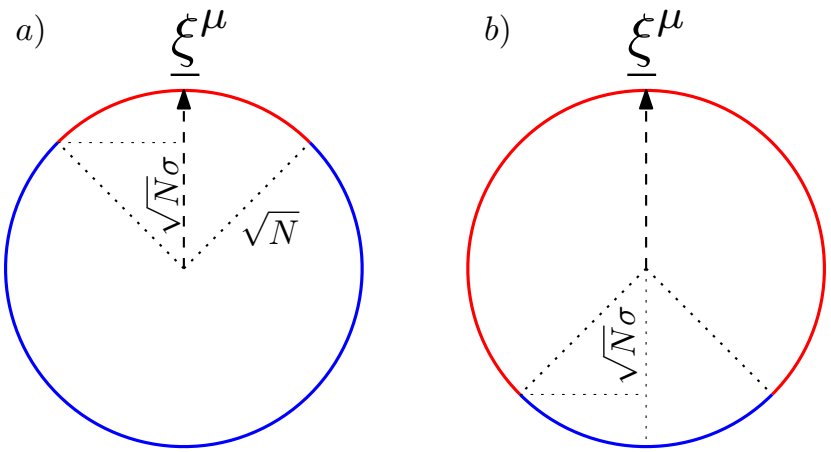


FIG. 9: Allowed phase space for a given pattern $\underline{\xi}^{\mu}$ for a) $\sigma > 0$ and b) $\sigma < 0$.

region is itself convex and therefore we deduce that the space of solution is formed by a unique convex cluster of phase space points.

Conversely, for $\sigma < 0$ the allowed phase space is the intersection of non convex regions and therefore it can be non convex too. In particular this intersection could give rise to disconnected islands of solutions.

Therefore, based on this consideration we can already figure out a glimps of the phase diagram of the model. Indeed for $\sigma > 0$ the CSP is not glassy at all while for $\sigma < 0$ glassy behavior can appear.

**The origin of the perceptron.** - The perceptron model was introduce in the context of machine learning as the simplest linear classifier [47]. In the original papers, one wanted to classify a given data set. Each element of a the data set is represented by a pattern $\underline{\xi}^{\mu}$. To each patter one assigns a label $\sigma^{\mu}$. We restrict to the case in which the labels are two, and therefore one could say that they are $\sigma^{\mu} = \pm 1$. Given the set of patterns and the set of labels corresponding to them, the perceptron problem is to find a set of weights $\underline{X}$ that separate the data set linearly into the two classes. This can be written as

$$\sigma^{\mu} = \mathrm{sgn}\left(\underline{\xi}^{\mu} \cdot x\right) \qquad \forall \mu = 1, \ldots, M \,. \tag{19}$$

This problem was extensively studied in the last thirty years [48–51]. Modern deep networks work with the same principle. Instead of having a linear function classifier, they are engineered in order to take into account for non linearities in the data set. However the building blocks of these architectures remain the perceptron.

### 5. *Further readings*

General books and reviews on the glass transition and structural glasses are [2, 3, 52–58].
Some classic papers on the random first order transition theory and spin glasses are [10, 19, 21, 33, 35, 59–62].
The solution of structural glass models in the high dimensional limit can be found in [25–31, 63, 64].
Some classic papers on the statistical physics of constraint satisfaction problems are [38–41, 65–67].

Finally a set of books is available on the relation between spin glasses, neural networks and machine learning [24, 34, 68–70]

## III. THE SPHERICAL RANDOM PERCEPTRON: THE REPLICA APPROACH

Here we start the study of the spherical random perceptron model. The content of this section has been published in [45, 46] and we will closely follow these two works explaining and clarifying many parts while introducing the main tools and techniques. Another interesting review paper close to what will be presented is [71].

In order to compute and analyze the space of solutions of the spherical random perceptron we can introduce a partition function [50]

$$Z_\xi = \int \mathcal{D}\underline{X}\, e^{-\beta H[\underline{X}]} = \int \mathcal{D}\underline{X}\, e^{-\frac{\beta}{2}\sum_{\mu=1}^{\alpha N} h_\mu(\underline{X})^2\theta(-h_\mu(\underline{X}))} \qquad h_\mu(\underline{X}) = \frac{1}{\sqrt{N}}\underline{\xi}^\mu\cdot\underline{X} - \sigma \tag{20}$$

and the measure $\mathcal{D}\underline{X}$ is the flat measure on the $N$ dimensional sphere $|\underline{X}|^2 = N$. The parameter $\beta = 1/T$ can be thought as the inverse temperature as usual and can be used to set the energy scale in the problem. For example setting the limit $\beta \to \infty$ allows to select the ground state. Note that this is a partition function for a disordered model since the patterns $\underline{\xi}^\mu$ play the role of quenched disorder.

As we have seen, the SAT/UNSAT transition can be strictly defined in the $N \to \infty$ limit. We are interested in computing whether, given a point in the $(\sigma, \alpha)$ plane, the problem is SAT or UNSAT. In the SAT phase, the total energy of the system is zero and therefore the partition function of Eq. (20) reduces to the volume of solutions of the CSP. Instead in the SAT phase, the partition function is dominated by the ground state configuration.

Given the partition function, we can compute the free energy of the model as

$$\mathrm{f}_\xi = -\lim_{N\to\infty}\frac{1}{N\beta}\ln Z_\xi\,. \tag{21}$$

Note that $\mathrm{f}_\xi$ depends explicitly on the disorder. However we are interested in what happens in the average case and therefore we introduce the averaged free energy given by

$$\mathrm{f} = -\lim_{N\to\infty}\frac{1}{N\beta}\overline{\ln Z_\xi} \tag{22}$$

where the overbar stands for the average over the random patterns $\{\underline{\xi}^\mu\}$.

The free energy can be decomposed, as usual, into two pieces

$$\mathrm{f} = e - Ts \tag{23}$$

being $e$ the average energy of the system and $s$ the entropy. Taking the $T \to 0$ limit, in the SAT phase the average free energy reduces to $\mathrm{f} \to -Ts$ and therefore one obtains that the entropy of solutions of the CSP is given by

$$s = -\lim_{\beta\to\infty}\beta\mathrm{f}\,. \tag{24}$$

Conversely, in the UNSAT phase, when $T \to 0$ the energy is finite and the system sits in a energy minimum and therefore $Ts \to 0$. Therefore the free energy tends to the ground state energy.

### 1. The replica approach to compute the free energy of the system

We want to compute the average free energy defined in Eq. (22). In order to do that we need to average the logarithm of the partition function over the distribution of the random patterns $\underline{\xi}^\mu$. In generic situations this is a difficult task. A possible solution to the problem is provided by the replica method [24]. This employs the following identity

$$\mathrm{f} = -\lim_{N\to\infty}\frac{1}{\beta N}\overline{\ln Z_\xi} = -\lim_{N\to\infty}\lim_{n\to 0}\frac{1}{\beta N}\partial_n \overline{Z_\xi^n} \tag{25}$$

The quantity $\overline{Z^n}$ can be computed easily in the case in which $n$ takes integer values. Indeed in this case we can represent $Z^n$ with a multidimensional integral over $n$ collective coordinates $\{\underline{X}^{(a)}\}_{a=1,\dots,n}$:

$$Z_\xi^n = \int\left[\prod_{a=1}^{n}\mathcal{D}\underline{X}^{(a)}\right]\exp\left[-\beta\sum_{a=1}^{n}H[\underline{X}^{(a)}]\right]. \tag{26}$$

One can look at $\{\underline{X}^{(a)}\}$ as the coordinates of a set of $n$ copies or *replicas* of the original system. All replicas feel the same disorder realization. Before performing the average over the random patterns we introduce the following notation

$$v(h) = \frac{1}{2}h^2\theta(-h)\,. \tag{27}$$

The average over the replicated partition function defined in Eq. (26) can be performed in the following way:

$$\overline{Z_\xi^n} = \overline{\int\left[\prod_{a=1}^{n}\mathcal{D}\underline{X}^{(a)}\left[\prod_{\mu=1}^{\alpha N}\mathrm{d}r_\mu^a\right]\right]\exp\left[-\beta\sum_{a=1}^{n}\sum_{\mu=1}^{\alpha N}v(r_\mu^{(a)}-\sigma)\right]\prod_{a=1}^{n}\prod_{\mu=1}^{\alpha N}\delta(r_\mu^{(a)}-\frac{1}{\sqrt{N}}\underline{\xi}^\mu\cdot\underline{X}^{(a)})}\,. \tag{28}$$

Using the Fourier representation for the Dirac deltas we get

$$\begin{aligned}\overline{Z_\xi^n} = \int\left[\prod_{a=1}^{n}\mathcal{D}\underline{X}^{(a)}\left[\prod_{\mu=1}^{\alpha N}\frac{\mathrm{d}r_\mu^a\mathrm{d}\hat{r}_\mu^{(a)}}{2\pi}\right]\right]\exp\left[-\beta\sum_{a=1}^{n}\sum_{\mu=1}^{\alpha N}v(r_\mu^{(a)}-\sigma)+\sum_{\mu=1}^{\alpha N}\sum_{a=1}^{n}i\hat{r}_\mu^{(a)}r_\mu^{(a)}\right]\\ \times\overline{\exp\left[-\frac{i}{\sqrt{N}}\sum_{\mu=1}^{\alpha N}\sum_{a=1}^{n}\hat{r}_\mu^{(a)}\underline{\xi}^\mu\cdot\underline{X}^{(a)}\right]}\,.\end{aligned} \tag{29}$$

We can now focus on the last line of the previous equation to perform the average over the random patterns

$$\overline{\exp\left[-\frac{i}{\sqrt{N}}\sum_{\mu=1}^{\alpha N}\sum_{a=1}^{n}\hat{r}_\mu^{(a)}\underline{\xi}^\mu\cdot\underline{X}^{(a)}\right]} = \exp\left[-\frac{1}{2N}\sum_{a,b=1}^{n}\sum_{\mu=1}^{\alpha N}\hat{r}_\mu^{(a)}\hat{r}_\mu^{(b)}\underline{X}^{(a)}\cdot\underline{X}^{(b)}\right]. \tag{30}$$

At this point we can observe that in Eq. (28) the $n$ replicas of the system were uncoupled. However after performing the average over the disorder they become interacting. Now we introduce the overlap matrix defined as

$$Q_{ab} = \frac{1}{N}\underline{X}^{(a)}\cdot\underline{X}^{(b)}. \tag{31}$$

The spherical constraint $|\underline{X}^{(a)}|^2 = N$ implies that $Q_{aa} = 1$ for all $a = 1,\dots,n$. $Q_{ab}$ is by definition a symmetric matrix and has a direct physical interpretation. Given two configurations $\underline{X}^{(a)}$ and $\underline{X}^{(b)}$ of two replicas, $a$ and

$b$, $Q_{ab}$ gives a measure of similarity between them. In particular $Q_{ab}=0$ if the two vectors $\underline{X}^{(a)}$ and $\underline{X}^{(b)}$ are orthogonal on the $N$ dimensional sphere. In this way the average replicated partition function is

$$\begin{aligned}\overline{Z_\xi^n} = \int\left(\prod_{a<b}\mathrm{d}Q_{ab}\right)\int\left[\prod_{a=1}^{n}\prod_{\mu=1}^{\alpha N}\frac{\mathrm{d}r_\mu^a\mathrm{d}\hat{r}_\mu^{(a)}}{2\pi}\right]\exp\left[-\beta\sum_{a=1}^{n}\sum_{\mu=1}^{\alpha N}v(r_\mu^{(a)}-\sigma)+\sum_{\mu=1}^{\alpha N}\sum_{a=1}^{n}i\hat{r}_\mu^{(a)}r_\mu^{(a)}\right]\\ \times\exp\left[-\frac{1}{2}\sum_{a,b=1}^{n}\sum_{\mu=1}^{\alpha N}\hat{r}_\mu^{(a)}\hat{r}_\mu^{(b)}Q_{ab}\right]\int\left[\prod_{a=1}^{n}\mathcal{D}\underline{X}^{(a)}\right]\left[\prod_{a\leq b}\delta\left(Q_{ab}-\frac{1}{N}\underline{X}^{(a)}\cdot\underline{X}^{(b)}\cdot\right)\right]\end{aligned} \tag{32}$$

At this point we would like to perform the integration over $\{\underline{X}^{(a)}\}$. This can be done in the following way.
**The Jacobian of the change of variables**[7]**.** - In order to compute the Jacobian of the change of variables from $\{\underline{X}^{(a)}\}$ to the matrix $Q$ we first rewrite

$$\begin{aligned}J(Q) &= \int\left[\prod_{a=1}^{n}\mathcal{D}\underline{X}^{(a)}\right]\left[\prod_{a\leq b}\delta\left(Q_{ab}-\frac{1}{N}\underline{X}^{(a)}\cdot\underline{X}^{(b)}\right)\right]\\ &= N^{n(n-1)/2}\int\left[\prod_{a=1}^{n}\mathcal{D}\underline{X}^{(a)}\right]\left[\prod_{a\leq b}\delta\left(NQ_{ab}-\underline{X}^{(a)}\cdot\underline{X}^{(b)}\right)\right].\end{aligned} \tag{33}$$

Then we consider the integral over $\{\underline{X}^{(a)}\}$. Note that since $Q_{aa}=1$ we can integrate freely the components of the vectors $\{\underline{X}^{(a)}\}$. Using the Fourier representation of the Dirac delta function we get

$$J(Q) = N^{n(n-1)/2}\int\prod_{a\leq b}\frac{\mathrm{d}\hat{Q}_{ab}}{2\pi}\int\left[\prod_{a=1}^{n}\mathrm{d}\underline{X}^{(a)}\right]\exp\left[iN\sum_{a\leq b}\hat{Q}_{ab}Q_{ab}-i\sum_{a\leq b}\hat{Q}_{ab}\underline{X}^{(a)}\cdot\underline{X}^{(b)}\right] \tag{34}$$

The integral over $\{\underline{X}^{(a)}\}$ becomes Gaussian and can be done explicitly:

$$\int\left[\prod_{a=1}^{n}\mathrm{d}\underline{X}^{(a)}\right]\exp\left[iN\sum_{a\leq b}\hat{Q}_{ab}Q_{ab}-i\sum_{a\leq b}\hat{Q}_{ab}\underline{X}^{(a)}\cdot\underline{X}^{(b)}\right] = (2\pi)^{Nn/2}\exp\left[-\frac{N}{2}\ln\det\tilde{Q}\right] \tag{35}$$

being

$$\tilde{Q} = i\left(1+\delta_{ab}\right)\hat{Q}_{ab}\,. \tag{36}$$

Therefore we get

$$J(Q) = N^{n(n-1)/2}\left(2\pi\right)^{Nn/2}\int\prod_{a\leq b}\frac{\mathrm{d}\hat{Q}_{ab}}{2\pi}\exp\left[iN\sum_{a\leq b}\hat{Q}_{ab}Q_{ab}-\frac{N}{2}\ln\det\tilde{Q}\right]. \tag{37}$$

The integral over $\hat{Q}$ can be performed via saddle point method. The saddle point equation gives

$$\tilde{Q} = Q^{-1} \tag{38}$$

and therefore

$$\begin{aligned}J(Q) &\simeq N^{n(n-1)/2}(2\pi)^{-n(n-1)/2}\exp\left[\frac{Nn}{2}(1+\ln(2\pi))+\frac{N}{2}\ln\det Q\right]\\ &= D_{N,n}\exp\left[\frac{Nn}{2}(1+\ln(2\pi))+\frac{N}{2}\ln\det Q\right]\end{aligned} \tag{39}$$

[7] An alternative way to perform this computation is given in [26].

being

$$D_{N,n} = N^{n(n-1)/2}(2\pi)^{-n(n-1)/2}\,. \tag{40}$$

Using the expression of the Jacobian of the change of variables we get that the replicated action becomes

$$\overline{Z_\xi^n} = D_{N,n}\int\left(\prod_{a<b}\mathrm{d}Q_{ab}\right)\exp\left[\frac{Nn}{2}\left(1+\ln(2\pi)\right)+\frac{N}{2}\ln\det Q+\alpha N\ln\mathcal{Z}\right] \tag{41}$$

where $\mathcal{Z}$ is given by

$$\mathcal{Z} = \int\left[\prod_{a=1}^{n}\frac{\mathrm{d}r^a\mathrm{d}\hat{r}^{(a)}}{2\pi}\right]\exp\left[-\beta\sum_{a=1}^{n}v(r^{(a)}-\sigma)+\sum_{a=1}^{n}i\hat{r}^{(a)}r^{(a)}-\frac{1}{2}\sum_{a,b=1}^{n}\hat{r}^{(a)}\hat{r}^{(b)}Q_{ab}\right]\,. \tag{42}$$

This is due to the fact that once averaged over the disorder, the integral over the variables $\{r_\mu^{(a)},\hat{r}_\mu^{(a)}\}$ is factorized in the constraint index $\mu$. This is the source of the $\alpha N$ proportionality factor in front of the term $\ln\mathcal{Z}$ in Eq. (41). At this point it is very useful to introduce the following identity

$$\exp\left[-\frac{1}{2}\sum_{a,b=1}^{n}Q_{ab}\hat{r}^{(a)}\hat{r}^{(b)}\right] = \exp\left[\frac{1}{2}\sum_{a,b=1}^{n}Q_{ab}\frac{\partial^2}{\partial h_a\partial h_b}\right]\left[\prod_{c=1}^{n}\exp\left[-i\hat{r}^{(c)}h_c\right]\right]\Bigg|_{\{h_c=0\}} \tag{43}$$

from which we can write

$$\begin{aligned}\mathcal{Z} &= \exp\left[\frac{1}{2}\sum_{a,b=1}^{n}Q_{ab}\frac{\partial^2}{\partial h_a\partial h_b}\right]\left[\prod_{c=1}^{n}\int\frac{\mathrm{d}r^c\mathrm{d}\hat{r}^{(c)}}{2\pi}\exp\left[-\beta v(r^{(c)}-\sigma)+i\hat{r}^{(c)}(r^{(c)}-h_c)\right]\right]\Bigg|_{\{h_c=0\}}\\ &= \exp\left[\frac{1}{2}\sum_{a,b=1}^{n}Q_{ab}\frac{\partial^2}{\partial h_a\partial h_b}\right]\left[\prod_{c=1}^{n}\exp\left[-\beta v(h_c-\sigma)\right]\right]\Bigg|_{\{h_c=0\}}\,.\end{aligned} \tag{44}$$

Therefore the average replicated partition function can be rewritten in the following way

$$\begin{aligned}\overline{Z_\xi^n} &= D_{N,n}\int\left(\prod_{a<b}\mathrm{d}Q_{ab}\right)\exp\left[N\mathcal{S}(Q)+\frac{Nn}{2}\left(1+\ln(2\pi)\right)\right]\\ \mathcal{S}(Q) &= \frac{1}{2}\ln\det Q+\alpha\ln\exp\left[\frac{1}{2}\sum_{a,b=1}^{n}Q_{ab}\frac{\partial^2}{\partial h_a\partial h_b}\right]\left[\prod_{c=1}^{n}\exp\left[-\beta v(h_c-\sigma)\right]\right]\Bigg|_{\{h_c=0\}}\,.\end{aligned} \tag{45}$$

We call $S(Q)$ the replicated action. We see that the replicated partition function has been finally expressed in terms of an integral over the $n\times n$ matrix $Q$.

Looking back at the free energy, Eq. (25) implies that

$$\begin{aligned}\mathrm{f} &= -\lim_{N\to\infty}\lim_{n\to 0}\frac{1}{\beta N}\partial_n\overline{Z^n}\\ &= -\lim_{N\to\infty}\lim_{n\to 0}\frac{1}{\beta N}\partial_n\left[D_{N,n}\int\left(\prod_{a<b}\mathrm{d}Q_{ab}\right)\exp\left[N\mathcal{S}(Q)+\frac{Nn}{2}\left(1+\ln(2\pi)\right)\right]\right]\,.\end{aligned} \tag{46}$$

At this point we exchange the limits in order to get

$$\mathrm{f} = -\lim_{n\to 0}\lim_{N\to\infty}\frac{1}{\beta N}\partial_n\left[D_{N,n}\int\left(\prod_{a<b}\mathrm{d}Q_{ab}\right)\exp\left[N\mathcal{S}(Q)+\frac{Nn}{2}\left(1+\ln(2\pi)\right)\right]\right]\,. \tag{47}$$

In the large $N$ limit, the integral over the matrix $Q$ can be evaluated using a saddle point approximation.

$$\int \left( \prod_{a<b} \mathrm{d}Q_{ab} \right) \exp\left[ N\mathcal{S}(Q) \right] \simeq \exp\left[ N\mathcal{S}(Q^*) \right] \tag{48}$$

where $Q^*$ is the solution of the saddle point equation

$$\frac{\partial \mathcal{S}(Q)}{\partial Q_{ab}} = 0\,. \tag{49}$$

Therefore the free energy becomes

$$\mathrm{f} = -\frac{T}{2}(1+\ln(2\pi)) - T\lim_{n\to 0}\partial_n \mathcal{S}(Q^*) \tag{50}$$

Note that we have supposed that $S(Q)$ is of the order $n$ for $n \to 0$ which is a reasonable assumption. In the UNSAT phase the constant $T(1+\ln(2\pi))/2$ is completely irrelevant since it goes to zero. In the SAT phase it gives a constant shift to the entropy of solutions. Therefore it is completely irrelevant.

Eq. (49) can be made explicit:

$$0 = \left[Q^{-1}\right]_{ab} + \alpha\beta^2 \frac{e^{\frac{1}{2}\sum_{l,m=1}^{n} Q_{lm}\frac{\partial^2}{\partial h_l \partial h_m}} v'(h_a)v'(h_b)\prod_{s=1}^{n} e^{-\beta v(h_s)}\Big|_{\{h_s=-\sigma\}}}{e^{\frac{1}{2}\sum_{l,m=1}^{n} Q_{lm}\frac{\partial^2}{\partial h_l \partial h_m}} \prod_{s=1}^{n} e^{-\beta v(h_s)}\Big|_{\{h_s=-\sigma\}}}\,. \tag{51}$$

Finding the solution of this saddle point equation is a difficult problem. The main difficulty arises because whatever is the solution at finite integer $n$, we need to consider an analytic continuation down to $n \to 0$. Since $n$ is the dimension of the symmetric matrix $Q$, one should find the saddle point solution of $n(n-1)/2$ parameters. It is completely not clear what means to take the analytic continuation of the number of parameters to zero. A possible solution of the problem would come if the saddle point elements of the matrix $Q$ are structured in such a way that if $S(Q)$ is computed within this structure it becomes an analytic function of $n$.

Therefore in order to solve the problem one could try to assume a particular form for $Q$ that is simple enough to allow $S(Q)$ to become an analytic function of $n$. The space of possible parametrizations that allow this is in principle huge and furthermore it could depend on the particular form of $S(Q)$.

Here we will assume that the matrix $Q$ has an ultrametric structure [24, 72, 73].

The first example of an ultrametric matrix $Q$ is a *replica symmetric* (RS) matrix. Therefore we will discuss first the RS solution and then we will generalize it to generic ultrametric matrices.

### A. The physical meaning of the overlap

Before entering into the parametrization of the overlap matrix $Q_{ab}$ we would like to discuss the physical meaning of this *order parameter* [10, 24, 74]. Let us consider two vectors $\underline{X}^{(1)}$ and $\underline{X}^{(2)}$ subjected to the same disorder $\{\underline{\xi}^{\mu}\}$ and therefore subjected to the same energy cost function. Given this we can ask what is the typical probability distribution of the overlap between the two once we extract them from the Boltzmann measure. More precisely we define

$$P_{\xi}(q) = \int \mathcal{D}\underline{X}^{(1)}\mathcal{D}\underline{X}^{(2)} \frac{e^{-\beta H[\underline{X}^{(1)}]}}{Z_{\xi}} \frac{e^{-\beta H[\underline{X}^{(2)}]}}{Z_{\xi}} \delta\left( q - \frac{1}{N}\underline{X}^{(1)}\cdot\underline{X}^{(2)} \right)\,. \tag{52}$$

This probability density depends on the disorder. We are interested in the typical behavior and therefore we define

$$\overline{P_\xi(q)} = \int \mathcal{D}\underline{X}^{(1)}\mathcal{D}\underline{X}^{(2)} \overline{\frac{e^{-\beta H[\underline{X}^{(1)}]}}{Z_\xi}\frac{e^{-\beta H[\underline{X}^{(2)}]}}{Z_\xi}} \delta\left(q - \frac{1}{N}\underline{X}^{(1)}\cdot\underline{X}^{(2)}\right) . \tag{53}$$

In order to average the normalization factors, we make use again of the replica method. We write

$$\begin{aligned} P(q) \equiv \overline{P_\xi(q)} &= \lim_{n\to 0}\int \mathcal{D}\underline{X}^{(1)}\mathcal{D}\underline{X}^{(2)} \overline{e^{-\beta H[\underline{X}^{(1)}]}e^{-\beta H[\underline{X}^{(2)}]}Z_\xi{}^{n-2}}\,\delta\left(q - \frac{1}{N}\underline{X}^{(1)}\cdot\underline{X}^{(2)}\right) \\ &= \lim_{n\to 0}\int \overline{\left[\prod_{a=1}^{n}\mathcal{D}\underline{X}^{(a)}e^{-\beta H[\underline{X}^{(a)}]}\right]}\,\delta\left(q - \frac{1}{N}\underline{X}^{(1)}\cdot\underline{X}^{(2)}\right) \\ &= \lim_{n\to 0}\frac{2}{n(n-1)}\sum_{a<b}\int \overline{\left[\prod_{a=1}^{n}\mathcal{D}\underline{X}^{(a)}e^{-\beta H[\underline{X}^{(a)}]}\right]}\,\delta\left(q - \frac{1}{N}\underline{X}^{(a)}\cdot\underline{X}^{(b)}\right) \\ &= \lim_{n\to 0}\frac{2}{n(n-1)}\sum_{a<b}\delta\left(q - Q_{ab}\right) \end{aligned} \tag{54}$$

being $Q_{ab}$ the saddle point value obtained by solving Eq. (49). Therefore the form of the saddle point solution of the overlap matrix encodes for the average probability distribution of the overlap. In the zero temperature limit and in the SAT phase, the overlap distribution tells us how far two typical solutions of the CSP are.

The line of reasoning that brought us to Eq. (54) is general. Furthermore we note that if the Hamiltonian has some global symmetry, this can be inherited by the overlap distribution. In particular when the spin up-down symmetry is satisfied, the overlap distribution is symmetric with respect to $q = 0$ [24].



### B. The replica symmetric solution

We can assume that the form of the saddle point solution of Eq. (51) is

$$Q_{ab} = \delta_{ab} + (1 - \delta_{ab})q\,. \tag{55}$$

This is a matrix that has the elements of the diagonal all equal to one, due to the spherical constraint, and equal to $q$ outside the diagonal. Assuming this form of the saddle point solution, we need to find the value of $q$ on the manifold of the RS matrices $Q$ that extremizes $S(Q)$. Therefore we first plug the RS ansatz of Eq. (55) inside the form of $S(Q)$. Let us first consider the term coming from the Jacobian of the change of variables. We have

$$\ln\det Q = \ln\left[(1-q)^{n-1}(1+(n-1)q)\right] = (n-1)\ln(1-q) + \ln(1+(n-1)q)\,. \tag{56}$$

We have now to evaluate the second term given by

$$\ln\mathcal{Z} = \alpha\ln\exp\left[\frac{1}{2}\sum_{a,b=1}^{n}Q_{ab}\frac{\partial^2}{\partial h_a\partial h_b}\right]\left[\prod_{c=1}^{n}\exp\left[-\beta v(h_c)\right]\right]\Bigg|_{\{h_c=-\sigma\}} \tag{57}$$

In order to do that we consider first the differential operator

$$\frac{1}{2}\sum_{a,b=1}^{n}Q_{ab}\frac{\partial^2}{\partial h_a\partial h_b} = \frac{q}{2}\left(\sum_{a=1}^{n}\frac{\partial}{\partial h_a}\right)^2 + \frac{1}{2}(1-q)\sum_{a=1}^{n}\frac{\partial^2}{\partial h_a^2} \tag{58}$$

from which we get

$$\ln \mathcal{Z} = \alpha \ln \exp\left[\frac{q}{2}\left(\sum_{a=1}^{n}\frac{\partial}{\partial h_a}\right)^2\right]\left[\prod_{c=1}^{n}\exp\left[\frac{1}{2}(1-q)\frac{\partial^2}{\partial h_c^2}\right]\exp\left[-\beta v(h_c)\right]\right]\Bigg|_{\{h_c=-\sigma\}} . \tag{59}$$

At this point we introduce the following identity

$$\exp\left[\frac{\omega}{2}\frac{\partial^2}{\partial h^2}\right] f(h) = \int_{-\infty}^{\infty}\frac{\mathrm{d}z}{\sqrt{2\pi\omega}} e^{-z^2/(2\omega)} f(h-z) \equiv \gamma_\omega \star f(h) \tag{60}$$

One way to prove this identity is by perturbation theory:

$$\exp\left[\frac{\omega}{2}\frac{\partial^2}{\partial h^2}\right] f(h) = \sum_{k=0}^{\infty}\frac{\omega^k}{2^k k!} f^{(2k)}(h) . \tag{61}$$

On the other end we have

$$\begin{aligned}\int_{-\infty}^{\infty}\frac{\mathrm{d}z}{\sqrt{2\pi\omega}} e^{-z^2/(2\omega)} f(h-z) &= \sum_{k=0}^{\infty}\int_{-\infty}^{\infty}\frac{\mathrm{d}z}{\sqrt{2\pi\omega}} e^{-z^2/(2\omega)}\frac{(-1)^k z^k}{k!} f^{(k)}(h) \\ &= \sum_{k=0}^{\infty}\frac{f^{(2k)}(h)}{(2k)!}\omega^k (2k-1)!! = \sum_{k=0}^{\infty}\frac{\omega^k}{2^k k!} f^{(2k)}(h)\end{aligned} \tag{62}$$

which is Eq. (61).

Therefore we have

$$\ln \mathcal{Z} = \alpha \ln \exp\left[\frac{q}{2}\left(\sum_{a=1}^{n}\frac{\partial}{\partial h_a}\right)^2\right]\left[\prod_{c=1}^{n}\gamma_{1-q}\star\exp\left[-\beta v(h_c)\right]\right]\Bigg|_{\{h_c=-\sigma\}} . \tag{63}$$

At this point we introduce another trivial identity. We have that [75]

$$\left(\sum_{a=1}^{n}\frac{\partial}{\partial h}\right)^k R(h_1,\ldots,h_k)\Bigg|_{\{h_c=h\}} = \frac{\partial^k}{\partial h^k} R(h,\ldots,h) \qquad \forall k . \tag{64}$$

Therefore we can write

$$\ln \mathcal{Z} = \alpha \ln \exp\left[\frac{q}{2}\frac{\partial^2}{\partial h^2}\right]\left[\gamma_{1-q}\star\exp\left[-\beta v(h)\right]\right]^n\Big|_{h=-\sigma} = \alpha \ln \gamma_q \star \left[\gamma_{1-q}\star\exp\left[-\beta v(h)\right]\right]^n|_{h=-\sigma} \tag{65}$$

and thus finally the expression of $S(Q)$ under the replica symmetric ansatz is

$$S(Q) = \frac{1}{2}\left[(n-1)\ln(1-q) + \ln(1+(n-1)q)\right] + \alpha \ln \gamma_q \star \left[\gamma_{1-q}\star\exp\left[-\beta v(h)\right]\right]^n|_{h=-\sigma} \tag{66}$$

Since we are interested in the $n \to 0$ limit we can write

$$S(Q) \simeq n\tilde{S}(Q) = n\left[\frac{1}{2}\ln(1-q) + \frac{1}{2}\frac{q}{1-q} + \alpha\gamma_q \star \ln \gamma_{1-q}\star\exp\left[-\beta v(h)\right]|_{h=-\sigma}\right] . \tag{67}$$

Finally the saddle point equation that fixes the value of $q$ is given by

$$\frac{q}{(1-q)^2} = \alpha \int \frac{\mathrm{d}z}{\sqrt{2\pi q}} e^{-(h)^2/(2q)}\left[\frac{\partial}{\partial h}\ln \gamma_{1-q}\star\exp\left[-\beta v(h-\sigma)\right]\right]^2 . \tag{68}$$

We want now to take the zero temperature limit. In order to do that we first consider back the physical meaning of the overlap matrix $Q_{ab}$. For $a \neq b$, we have that

$$Q_{ab} = \lim_{N\to\infty} \frac{1}{N} \overline{\left\langle \underline{X}^{(a)} \cdot \underline{X}^{(b)} \right\rangle} \tag{69}$$

and the brackets indicate, in the zero temperature limit, the flat average over the solutions of the CSP. Therefore, in the SAT phase we can measure the typical distance of two random solutions of the CSP using the overlap. In particular the saddle point value of $q$ tells us that within the RS ansatz, all solution are in a unique cluster in which two typical solutions are at (co-)distance $q$. Furthermore if we are far away from the SAT/UNSAT threshold, the CSP has many distinct solutions and therefore $q < 1$. In this case we can easily take the zero temperature limit of Eq. (68) to get

$$\frac{q}{(1-q)^2} = \alpha \int \frac{\mathrm{d}z}{\sqrt{2\pi q}} e^{-h^2/(2q)} \left[ \frac{\partial}{\partial h} \ln \gamma_{1-q} \star \theta(h-\sigma) \right]^2 \tag{70}$$

where we have used the fact that

$$\lim_{\beta\to\infty} e^{-bv(h)} = \theta(h) \,. \tag{71}$$

Note that Eq. (70) is not sensible to the precise form of $v(h)$ in the sense that it does not depend on the precise form of the cost function for violated constraints. Finally we have that

$$\begin{aligned} \gamma_{1-q} \star \theta(h) &= \frac{1}{2} \left( 1 + \mathrm{erf}\left( \frac{h}{\sqrt{2(1-q)}} \right) \right) \equiv \Theta\left[ \frac{h}{\sqrt{2(1-q)}} \right] \\ \Theta(x) &= \frac{1}{2} \left( 1 + \mathrm{erf}(x) \right) \,. \end{aligned} \tag{72}$$



### 1. *The jamming transition at the RS level*

At this point we are equipped to study the SAT/UNSAT threshold within the RS ansatz. As we already discussed, $q$ is the typical co-distance between two solutions of the CSP. This is a function of $\sigma$ and $\alpha$. Changing the parameters, for example increasing the number of constraints by increasing $\alpha$, at fixed $\sigma$, one moves towards regions of the phase diagram where it becomes harder to find a SAT solution. Coming closer to the SAT/UNSAT threshold, the volume of solutions shrinks to zero. Therefore at the SAT/UNSAT transition where just one solution is present (at the RS level) the typical overlap between solutions goes to one. Therefore the SAT/UNSAT threshold can be computed by computing for which $\alpha$ Eq. (70) admits a solution $q \to 1$. Practically we can plug $q \to 1$ in Eq. (70) and this becomes an equation for the SAT/UNSAT threshold $\alpha_J(\sigma)$.

In the end we get

$$\alpha_J(\sigma) = \left[ \int_{-\infty}^{0} \frac{\mathrm{d}h}{\sqrt{2\pi}} e^{-(h+\sigma)^2/2} h^2 \right]^{-1} \,. \tag{73}$$

Another way to check that this is the correct SAT/UNSAT threshold within the RS ansatz is by computing the entropy of solutions. Indeed it turns out that

$$s \simeq \frac{1}{2} \ln(1-q) \to -\infty \qquad\qquad q \to 1 \tag{74}$$

and therefore the space of solutions reduces to one point when going close to the jamming transition line.

### 2. The UNSAT phase

In the UNSAT phase the system is in a minimum of the energy at zero temperature. Therefore in absence of thermal fluctuations $q \to 1$. However for infinitesimal temperatures, one can try a solution with

$$q \simeq 1 - \chi T \tag{75}$$

being $\chi$ a constant.

Plugging this ansatz inside Eq. (68) we get

$$\frac{1}{\chi^2 T^2} = \alpha \int \frac{\mathrm{d}z}{\sqrt{2\pi}} e^{-h^2/2} \left[ \frac{\partial}{\partial h} \ln \gamma_{\chi T} \star \exp\left[ -\frac{1}{T} v(h-\sigma) \right] \right]^2 \tag{76}$$

In order to take the zero temperature limit of the left hand side we look at

$$\ln \gamma_{\chi T} \star \exp\left[ -\frac{1}{T} v(h) \right] = \ln \int_{-\infty}^{\infty} \frac{\mathrm{d}z}{\sqrt{2\pi\chi T}} e^{-(h-z)^2/(2T\chi) - z^2\theta(-z)/(2T)} \; ; \tag{77}$$

for $T \to \infty$ and $h \sim \mathcal{O}(1)$ one can evaluate the integral by saddle point method. The saddle point equation through which $z$ is fixed is given by

$$\frac{z-h}{\chi} + z\theta(-z) = 0 \tag{78}$$

and therefore the solutions are

$$z^*(h) = \begin{cases} h & \text{for } h > 0 \\ \frac{h}{1+\chi} & \text{for } h < 0 \end{cases} \tag{79}$$

Plugging this solution inside Eq. (77) we get

$$\begin{aligned} \gamma_{\chi T} \star \exp\left[ -\frac{1}{T} v(h) \right] &= \ln \left[ \theta(h) \int_{-\infty}^{\infty} \frac{\mathrm{d}t}{\sqrt{2\pi\chi T}} e^{-t^2/(2\chi T)} + \theta(-h) e^{-h^2/(2(1+\chi)T)} \int_{-\infty}^{\infty} \frac{\mathrm{d}t}{\sqrt{2\pi\chi T}} e^{-\frac{1+\chi}{2\chi T} t^2} \right] \\ &\simeq \left( -\frac{h^2}{2(1+\chi)T} - \frac{1}{2}\ln(1+\chi) \right) \theta(-h) \; . \end{aligned} \tag{80}$$

Therefore Eq. (76) becomes

$$\frac{1+\chi^2}{\chi^2} = \alpha \int_{-\infty}^{0} \frac{\mathrm{d}h}{\sqrt{2\pi}} e^{-(h+\sigma)^2/2} h^2 \qquad \leftrightarrow \qquad \left( 1 + \frac{1}{\chi} \right)^2 = \frac{\alpha}{\alpha_J(\sigma)} \; . \tag{81}$$

This equation can be used to obtain the SAT/UNSAT transition coming from the UNSAT phase. Indeed since at unjamming, $q$ becomes smaller than 1, we should have that $\chi \to \infty$ for $\alpha \to \alpha_J(\sigma)$. Taking the $\chi \to \infty$ limit of Eq. (81) we get that the jamming line is given by Eq. (73). Once we enter in the UNSAT phase the energy of the system becomes different from zero because we have a finite fraction of unsatisfied constraints. In the zero temperature limit, the ground state of the system is obtained by taking the zero temperature limit of the free energy. Therefore within the RS approximation we have

$$e_{GS} = \lim_{T \to 0} \mathrm{f} = -\frac{1}{2\chi} + \frac{\alpha}{1+\chi} \int_{-\infty}^{\sigma} \frac{\mathrm{d}h}{\sqrt{2\pi}} e^{-h^2/2} \left( h - \sigma \right)^2 \; . \tag{82}$$

### 3. Gap distribution and the number of contacts

We have already defined a gap variable in Eq. (14). Let us consider its probability distribution. We define

$$\hat{\rho}_\xi(h) = \frac{1}{M}\sum_{\mu=1}^{M}\delta\left(h - h_\mu(\underline{X})\right) \ . \tag{83}$$

The gap distribution is therefore defined as

$$\rho(h) = \overline{\langle\hat{\rho}_\xi(h)\rangle} \tag{84}$$

where as usual the brackets stand for the Boltzmann average and the overline stands for the average over the disorder. In order to compute $\rho(h)$ we get back to the definition of the free energy

$$\mathrm{f} = -\lim_{N\to\infty}\frac{1}{\beta N}\overline{\ln Z_\xi} = -\lim_{N\to\infty}\frac{1}{\beta N}\overline{\ln\int\mathcal{D}\underline{X}e^{-\beta\sum_{\mu=1}^{M}v(h_\mu(\underline{X}))}} = -\lim_{N\to\infty}\frac{1}{\beta N}\overline{\ln\int\mathcal{D}\underline{X}e^{-\beta M\int \mathrm{d}h\hat{\rho}_\xi(h)v(h)}}. \tag{85}$$

Therefore we have

$$\frac{\delta\mathrm{f}}{\delta v(h)} = \overline{\frac{1}{Z_\xi}\int\mathcal{D}\underline{X}e^{-\beta H[\underline{X}]}\hat{\rho}(h)} = \rho(h)\,. \tag{86}$$

The free energy f at the replica symmetric level is given by

$$\mathrm{f} = -\frac{T}{2}\left(1+\ln(2\pi)\right) + \frac{1}{2}\left[\ln(1-q) + \frac{q}{1-q}\right] + \alpha\gamma_q\star\ln\gamma_{1-q}\star e^{-\beta v(\hat{h})}\Big|_{\hat{h}=-\sigma} \tag{87}$$

where $q$ is fixed to its saddle point value. Taking the functional derivative with respect to $v(h)$ we get

$$\begin{aligned}
\rho(h) &= \alpha\frac{\delta}{\delta v(h)}\ \alpha\gamma_q\star\ln\gamma_{1-q}\star e^{-\beta v(\hat{h})}\Big|_{\hat{h}=-\sigma} \\
&= \alpha\frac{\delta}{\delta v(h)}\int\frac{\mathrm{d}z}{\sqrt{2\pi q}}e^{-z^2/(2q)}\ln\int\frac{\mathrm{d}y}{\sqrt{2\pi(1-q)}}e^{-y^2/(2(1-q))}e^{-\beta v(-\sigma+z+y)} \\
&= \alpha\int\frac{\mathrm{d}z}{\sqrt{2\pi q}}e^{-z^2/(2q)}\frac{\int\frac{\mathrm{d}y}{\sqrt{2\pi(1-q)}}e^{-y^2/(2(1-q))}e^{-\beta v(-\sigma+z+y)}\delta(h+\sigma-z-y)}{\int\frac{\mathrm{d}y}{\sqrt{2\pi(1-q)}}e^{-y^2/(2(1-q))}e^{-\beta v(z-y)}} \\
&= \alpha\int\frac{\mathrm{d}z}{\sqrt{2\pi q}}e^{-(z+\sigma)^2/(2q)}\exp\left[-\beta v(h) - \frac{(h-z)^2}{2(1-q)} - f(1,z)\right]
\end{aligned} \tag{88}$$

where we have defined

$$f(1,h) = \ln\int\frac{\mathrm{d}y}{\sqrt{2\pi(1-q)}}e^{-y^2/(2(1-q))}e^{-\beta v(z-y)} \tag{89}$$

Starting from this and taking the jamming limit it can be shown that the number of contacts at the SAT/UNSAT threshold is

$$z = \Theta\left[\frac{\sigma}{\sqrt{2}}\right] \ . \tag{90}$$

It is interesting to compare the total number of contacts with the total number of degrees of freedom. The total number of contacts is $Mz = \alpha N z$. Instead the total number of degrees of freedom is $N$. We say that the system is

- hypostatic if $\alpha N z < N \implies \alpha z < 1$;
- isostatic if $\alpha N z = N \implies \alpha z = 1$;
- hyperstatic if $\alpha N z > N \implies \alpha z > 1$;

Therefore we can define an isostaticity index as $c = \alpha z$. For $\sigma > 0$, the system is hypostatic at jamming and becomes isostatic when $\sigma \to 0^+$. In the next sections we will see that jamming is isostatic in the non-convex region.

#### *4. Back to hard spheres*

It is interesting to go back to the analogy with the hard sphere model. Let us consider an amorphous jammed packings of hard spheres. At jamming there is a force network between spheres in contact that make the system solids and rigid.

The total number of degrees of freedom for a system with $N$ spheres and $d$ dimensions is $N_d = dN$. However, at jamming we have a contact network of constraints: spheres that touch cannot overlap. Therefore the total number of constraints that are *marginally satisfied*[8] is $N_c = zN/2$ where $z$ now is the average degree distribution of the contact network.

Mechanical stability of the packing requires that

$$N_c \geq N_d \implies \frac{zN}{2} \geq Nd \implies z \geq 2d\,. \tag{91}$$

This argument is due to Maxwell and implies that the average degree of the contact network is at least $2d$. Therefore stable packings are isostatic or hyperstatic. In numerical simulations it is found that amorphous jammed packings produced with different protocols are always isostatic and therefore are in a marginal situation. For this reason they are said to be marginally stable. Isostaticity has a deep impact on the *critical* properties of these systems and control many physical processes as for example avalanches and the vibrational spectrum. A review on the subject is [16].



### C. Stability of the replica symmetric solution: the de Almeida-Thouless transition

In the previous section we have assumed a replica symmetric form of the saddle point solution for the matrix $Q$. However since we are computing the saddle point we need to check that the solution we get is at least stable against small fluctuations. In other words, if we assume to expand $\mathcal{S}(Q)$ around the saddle point value, we should see a local maximum. The expansion of $\mathcal{S}(Q)$ is given by

$$\begin{aligned} \mathcal{S}(Q) &= \mathcal{S}(Q^*) + \frac{1}{2}\sum_{a<b}\sum_{c<d} M_{ab;cd}\delta Q_{ab}\delta Q_{cd} \\ &= \mathcal{S}(Q^*) + \frac{1}{8}\sum_{a\neq b}\sum_{c\neq d} \tilde{M}_{ab;cd}\delta Q_{ab}\delta Q_{cd} \end{aligned} \tag{92}$$

[8] In the sense that the spheres touch.

where $\delta Q_{ab} = Q_{ab} - Q^*_{ab}$ being $Q^*_{ab}$ the RS saddle point solution, and

$$M_{ab;cd} = \left.\frac{\delta^2 \mathcal{S}(Q)}{\delta Q_{ab}\delta Q_{cd}}\right|_{Q=Q^*} \tag{93}$$

Note that in Eq. (92) we have defined $\tilde{M}$ has the symmetrized version of $M$. A bit of reflection shows that due to the replica symmetric structure of the saddle point solution the operator $\tilde{M}$ has the following form

$$\tilde{M}_{ab;cd} = H_1 \frac{\delta_{ac}\delta_{bd} + \delta_{ad}\delta_{bc}}{2} + H_2 \frac{\delta_{ac} + \delta_{bd} + \delta_{ad} + \delta_{bc}}{4} + H_3 \,. \tag{94}$$

Indeed there are only three kinds of possible terms. They are

$$R_{1212} = \left.\frac{\delta^2 \mathcal{S}(Q)}{\delta Q_{12}\delta Q_{12}}\right|_{Q=Q^*} \qquad R_{1213} = \left.\frac{\delta^2 \mathcal{S}(Q)}{\delta Q_{12}\delta Q_{13}}\right|_{Q=Q^*} \qquad R_{1234} = \left.\frac{\delta^2 \mathcal{S}(Q)}{\delta Q_{12}\delta Q_{34}}\right|_{Q=Q^*} \tag{95}$$

and are connected to $H_1$, $H_2$ and $H_3$ by

$$\begin{cases} R_{1212} &= \frac{H_1}{2} + \frac{H_2}{2} + H_3 \\ R_{1213} &= \frac{H_3}{4} + H_3 \\ R_{1212} &= H_3 \end{cases} \implies \begin{cases} H_1 &= 2\left(R_{1212} - 2R_{1213} + R_{1234}\right) \\ H_2 &= 4\left(R_{1213} - R_{1234}\right) \\ H_3 &= R_{1234} \end{cases} \tag{96}$$

The stability of the replica symmetric solution requires that the quadratic form

$$\frac{1}{8}\sum_{a\neq b}\sum_{c\neq d} \tilde{M}_{ab;cd}\delta Q_{ab}\delta Q_{cd} \tag{97}$$

is at least semidefinite negative [76, 77]. In order to check it we first introduce the entropic and interaction terms given respectively by

$$\begin{aligned} \mathcal{S}_E(Q) &= \frac{1}{2}\ln\det Q \\ \mathcal{S}_I(Q) &= \alpha \ln \exp\left[\frac{1}{2}\sum_{l,m=1}^{n} Q_{lm}\frac{\partial^2}{\partial h_l \partial h_m}\right]\prod_{s=1}^{n} e^{-\beta v(h)}\Bigg|_{\underline{h}=-\sigma} \end{aligned} \tag{98}$$

and we will compute separately the elements of $\tilde{M}$ coming from them. In this section we will assume that we are in the SAT phase so that $e^{-\beta v(h)} \to \theta(h)$.

### 1. *Stability matrix: the entropic term*

We have to compute

$$\begin{aligned} R^{(E)}_{1212} &= \frac{\delta^2 \mathcal{S}_E(Q)}{\delta Q_{12}^2} = -\left[\left(Q^{-1}\right)_{11}\left(Q^{-1}\right)_{22} + \left(Q^{-1}\right)_{12}^2\right] \\ R^{(E)}_{1213} &= \frac{\delta^2 \mathcal{S}_E(Q)}{\delta Q_{12}\delta Q_{13}} = -\left[\left(Q^{-1}\right)_{11}\left(Q^{-1}\right)_{23} + \left(Q^{-1}\right)_{13}\left(Q^{-1}\right)_{23}\right] \\ R^{(E)}_{1234} &= \frac{\delta^2 \mathcal{S}_E(Q)}{\delta Q_{12}\delta Q_{34}} = -\left[\left(Q^{-1}\right)_{13}\left(Q^{-1}\right)_{24} + \left(Q^{-1}\right)_{14}\left(Q^{-1}\right)_{23}\right] \,. \end{aligned} \tag{99}$$

Since we need to compute these derivatives on the RS saddle point we need to find the inverse of a replica symmetric matrix. This is given by

$$Q_{ab} = (1-q)\delta_{ab} + q \implies \left(Q^{-1}\right)_{ab} = \frac{1}{1-q}\delta_{ab} - \frac{q}{(1-q)^2} \qquad n \to 0 \,. \tag{100}$$

Using this expression we get in the $n \to 0$ limit

$$\begin{aligned} H_1^{(E)} &= -\frac{2}{(1-q)^2} \\ H_2^{(E)} &= \frac{4q}{(1-q)^3} \\ H_3^{(E)} &= -\frac{2q^2}{(1-q)^4} \end{aligned} \tag{101}$$

which completes the entropic contribution to the stability matrix.

### 2. *Stability matrix: the interaction term*

We turn now to the computation of the terms of the stability matrix that come from the interaction term. Let us first consider

$$T^{(1)}_{1212} = \frac{\delta^2 S(Q)}{\delta Q^2_{12}} = \alpha \frac{\delta^2}{\delta Q^2_{12}} \exp\left[\frac{1}{2}\sum_{a,b=1}^{n} Q_{ab}\partial_a\partial_b\right] \prod_{s=1}^{n} \theta(h_s - \sigma)\Big|_{\underline{h}=0} = \alpha\left[\langle \partial_1^2\partial_2^2\rangle - \langle \partial_1\partial_2\rangle^2\right] \tag{102}$$

where we have defined

$$\langle \bullet \rangle = \frac{\exp\left[\frac{1}{2}\sum_{a,b=1}^{n} Q_{ab}\partial_a\partial_b\right] \bullet \prod_{s=1}^{n}\theta(h_s-\sigma)\Big|_{\underline{h}=0}}{\exp\left[\frac{1}{2}\sum_{a,b=1}^{n} Q_{ab}\partial_a\partial_b\right] \prod_{s=1}^{n}\theta(h_s-\sigma)\Big|_{\underline{h}=0}} \,. \tag{103}$$

The denominator of the expression above can be easily computed using the same steps as before. Using the replica symmetric form of the saddle point solution we get

$$\exp\left[\frac{1}{2}\sum_{a,b=1}^{n} Q_{ab}\partial_a\partial_b\right] \prod_{s=1}^{n}\theta(h_s-\sigma)\Big|_{\underline{h}=0} = \gamma_q \star \left[\gamma_{1-q} \star \exp\left[-\beta v(h)\right]\right]^n\big|_{h=-\sigma} \to 0 \qquad n \to 0\,. \tag{104}$$

Moreover we can compute

$$\begin{aligned} \langle \partial_1^2\partial_2^2\rangle &= \exp\left[\frac{1}{2}\sum_{a,b=1}^{n} Q_{ab}\partial_a\partial_b\right] \partial_1^2\theta(h_1-\sigma)\partial_2^2\theta(h_2-\sigma)\prod_{s=3}^{n}\theta(h_s-\sigma)\Big|_{\underline{h}=0} = \\ &= \exp\left[\frac{q}{2}\frac{\partial^2}{\partial h^2}\right]\left(\frac{\partial^2}{\partial h^2}\gamma_{1-q}\star\theta(h-\sigma)\right)^2\left(\gamma_{1-q}\star\theta(h-\sigma)\right)^{n-2}\Big|_{h=0} \\ &\to \int \frac{\mathrm{d}z}{\sqrt{2\pi q}} e^{-z^2/(2q)} \frac{g''(1,h-\sigma)}{g(1,h-\sigma)} \qquad n\to 0 \end{aligned} \tag{105}$$

where $g''(1,h) = \partial_h^2 g(1,h)$ and we have defined

$$g(1,h) \equiv \gamma_{1-q}\star\theta(h) = \Theta\left[\frac{h}{\sqrt{2(1-q)}}\right] \,. \tag{106}$$

Using this for all the other terms and defining

$$\langle \bullet \rangle_q = \int_{-\infty}^{\infty} \frac{\mathrm{d}z}{\sqrt{2\pi q}} e^{-(z+\sigma)^2/(2q)} \bullet \tag{107}$$

we have

$$
\begin{aligned}
T^{(I)}_{1212} &= \alpha \left[ \left\langle \left( \frac{g''(1,h)}{g(1,h)} \right)^2 \right\rangle_q - \left\langle \left( \frac{g'(1,h)}{g(1,h)} \right)^2 \right\rangle_q^2 \right] \\
T^{(I)}_{1213} &= \alpha \left[ \left\langle \frac{g''(1,h)}{g(1,h)} \left( \frac{g'(1,h)}{g(1,h)} \right)^2 \right\rangle_q - \left\langle \left( \frac{g'(1,h)}{g(1,h)} \right)^2 \right\rangle_q^2 \right] \\
T^{(I)}_{1234} &= \alpha \left[ \left\langle \left( \frac{g'(1,h)}{g(1,h)} \right)^4 \right\rangle_q - \left\langle \left( \frac{g'(1,h)}{g(1,h)} \right)^2 \right\rangle_q^2 \right]
\end{aligned}
\tag{108}
$$

Therefore the contribution of the interaction term to the stability matrix is given by

$$
\begin{aligned}
H^{(I)}_1 &= \alpha \left\langle \left( \frac{\partial^2}{\partial h^2} \ln g(1,h) \right)^2 \right\rangle_q \\
H^{(I)}_2 &= 4\alpha \left[ \left\langle \frac{g''(1,h)}{g(1,h)} \left( \frac{g'(1,h)}{g(1,h)} \right)^2 \right\rangle_q - \left\langle \left( \frac{g'(1,h)}{g(1,h)} \right)^4 \right\rangle_q \right] \\
H^{(I)}_3 &= \alpha \left[ \left\langle \left( \frac{g'(1,h)}{g(1,h)} \right)^4 \right\rangle_q - \left\langle \left( \frac{g'(1,h)}{g(1,h)} \right)^2 \right\rangle_q^2 \right]
\end{aligned}
\tag{109}
$$

This completes the computation of the contribution of the interaction term to the stability matrix. Having Eq. (101) and Eq. (109) one can easily compute the full expressions of $H_1$, $H_2$ and $H_3$.

#### 3. *The replicon eigenvalue*

It turns out that there is an eigenvalue of the stability matrix that becomes unstable in a certain region of the phase diagram. This wigenvalue is characterized by an eigenvector of the form

$$
\delta_R Q_{ab} : \qquad \sum_{b(\neq a)} \delta_R Q_{ab} = 0 \qquad \sum_{a(\neq b)} \delta_R Q_{ab} = 0 \tag{110}
$$

This subspace of fluctuations of the overlap matrix is usually called the *replicon* subspace and the associated eigenvalue is the replicon eigenvalue. Its expression (in the $n \to 0$ limit) is given by

$$
\lambda_R = M_1 = -2 \left[ \frac{1}{(1-q)^2} - \alpha \left\langle \left( \frac{\partial^2}{\partial h^2} \ln g(1,h) \right)^2 \right\rangle_q \right] \tag{111}
$$

Coming from the SAT phase and reaching the jamming line, this eigenvalue is always stable for $\sigma > 0$. Therefore we conclude that the jamming transition of the spherical random perceptron in the convex region of the phase diagram is replica symmetric. Instead, for $\sigma < 0$, the replicon eigenvalue becomes unstable before reaching the jamming transition and therefore in the non convex region, jamming is always in a region where the replica symmetric solution is unstable. Therefore in order to study the properties of the SAT/UNSAT threshold for $\sigma < 0$ we need to understand how to go beyond the replica symmetric ansatz.

### D. Replica symmetry breaking and its meaning

Replica symmetry breaking (RSB) was first discovered in the context of the Sherrington-Kirkpatrick model [78]. After it was understood that the replica symmetric solution was wrong at low temperature, some attempts

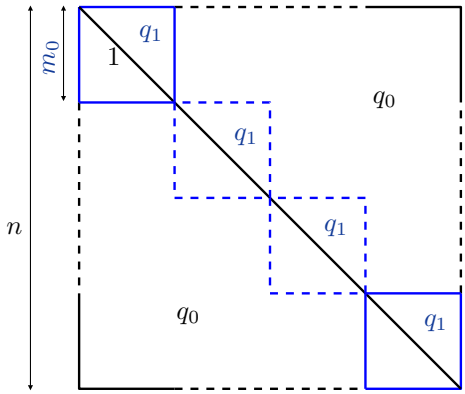


FIG. 10: The 1RSB structure of the overlap matrix

have been tried to go beyond the replica symmetric assumption [79]. The final and correct picture came out from a series of works by Parisi who constructed an iterative scheme of replica symmetry breaking. Parisi's solution of the Sherrington-Kirkpatrick model is now proven to be exact by a series of more recent mathematical proofs [80–83]. Despite the fact that it is not clear if these proofs can be adapted to the spherical random perceptron, we will conjecture that such RSB scheme applies also to this case and we will investigate its consequences.



### 1. *Parisi's replica symmetry breaking scheme*

In this section we describe the iterative scheme of RSB originally proposed by Parisi for the form of the overlap matrix. This is based on so called *hierarchical matrices*. Let us start from the simplest hierarchical matrix that is a replica symmetric one. In this case the matrix has a diagonal equal to one, the spherical constraint, and all the off-diagonal elements are equal to $q_0$.

The one-step replica symmetry breaking (1RSB) overlap matrix instead is obtained by dividing the group of $n$ replicas into $n/m_0$ subgroups of size $m_0$ each. This is illustrated in Fig. (10). The diagonal of the overlap matrix is always fixed to one due to the spherical constraint. The off-diagonal elements in the diagonal blocks are instead equal to $q_1$ while the elements outside the diagonal blocks are all equal to $q_0$. Therefore the 1RSB form of the overlap matrix is parametrized by three numbers: $m_0$, $q_0$ and $q_1$.

The two-step replica symmetry breaking (2RSB) form of $Q$ is obtained starting from the 1RSB one. This is illustrated in Fig. (11). In diagonal blocks of size $m_0$, sub-diagonal blocks of size $m_1$ appear. The off-diagonal elements of each sub-block are all equal to $q_2$ while the off diagonal elements outside the sub-blocks are left unchanged. Therefore the 2RSB ansatz is parametrized by five parameters: $m_0$, $m_1$, $q_0$, $q_1$, and $q_2$.

It is clear that this construction can be iterated. In order to construct a $k$RSB form of $Q$ one starts from the $(k-1)$RSB representation and takes the innermost diagonal blocks. Each of them undergoes the same process. New diagonal blocks of size $m_{k-1}$ are created and the off-diagonal elements belonging to them are given the value $q_k$. All the other elements of the overlap matrix are left unchanged.

Hierarchical matrices of this kind form an algebra. Let us consider two hierarchical matrices $A$ and $B$. We write

$$A \equiv \{A_d, \{A_i\}_{i=0,\dots,k}\} \qquad B \equiv \{B_d, \{B_i\}_{i=0,\dots,k}\} \tag{112}$$

being $A_d$ and $B_d$ the diagonal elements and the sets $\{A_i\}_{i=0,\dots,k}$ and $\{B_i\}_{i=0,\dots,k}$ the sets of parameters fixing

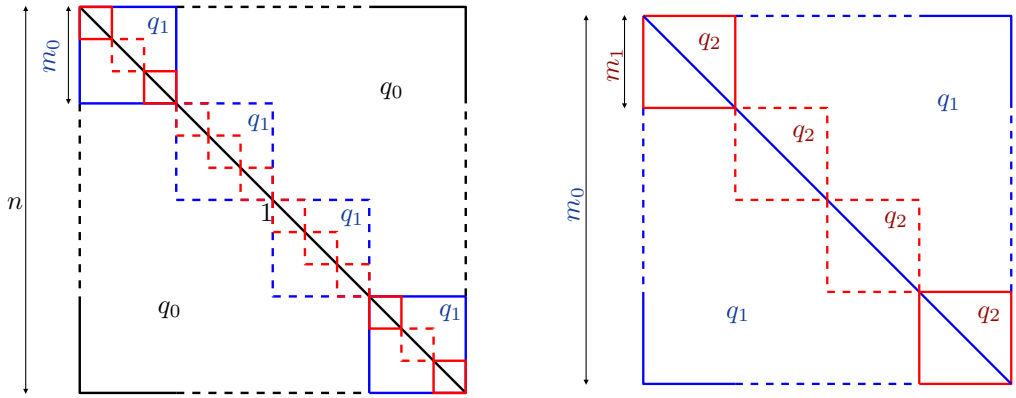


FIG. 11: The construction of the 2RSB structure of the overlap matrix starting from the 1RSB one. Each diagonal block undergoes to the same transformation with the same parameters.

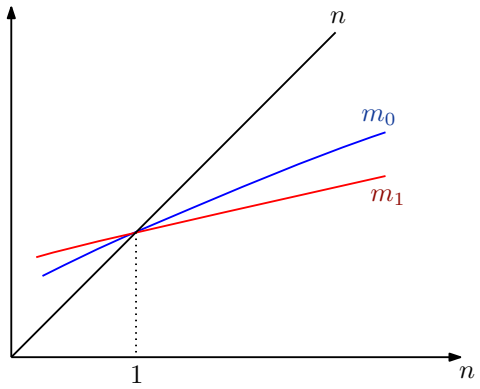


FIG. 12: The analytic continuation of $n \to 0$ that heuristically justify Eq. (114).

the $k$RSB structure. If we assume that both $A$ and $B$ have the same set of parameters $\{m_i\}_{i=0,\dots,k-1}$ then the product $C = AB = BA$ is a $k$RSB matrix and therefore $k$RSB matrices form an algebra.

We note now that by construction we have that

$$n > m_0 > m_1 > \ldots > m_{k-1} > m_k = 1 \tag{113}$$

However we want to take the $n \to 0$ limit. Therefore we need to reverse the inequalities signs of (113) to get

$$n < m_0 < m_1 < \ldots < m_{k-1} < m_k = 1 \tag{114}$$

A simple but still heuristic justification for this is represented in Fig. (12).

In the $n \to 0$ limit one can represent the parameters $\{q_i\}$ in a stepwise function as in Fig. (13-left). Therefore for $n \to 0$ the overlap can be represented as a stepwise function $q(x)$. In this way the $k \to \infty$ limit can be taken and the function $q(x)$ becomes continuous as represented in FIg. (13-right).

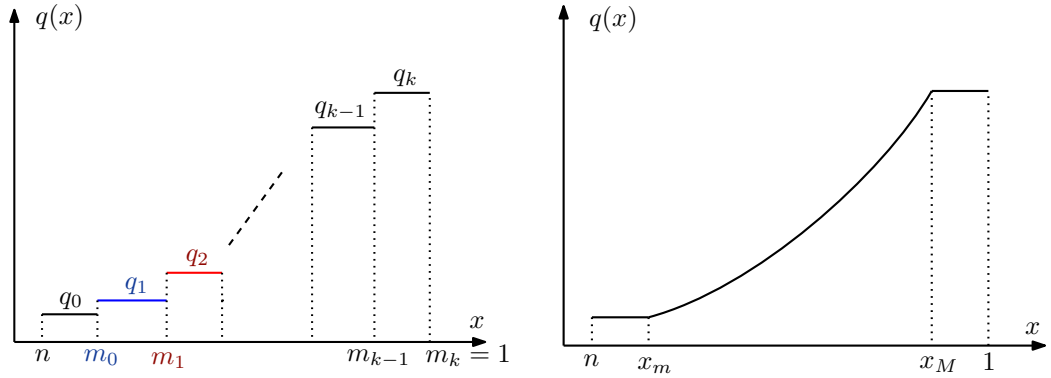


FIG. 13: The function $q(x)$ in a $k$RSB ansatz and in its continuous limit.

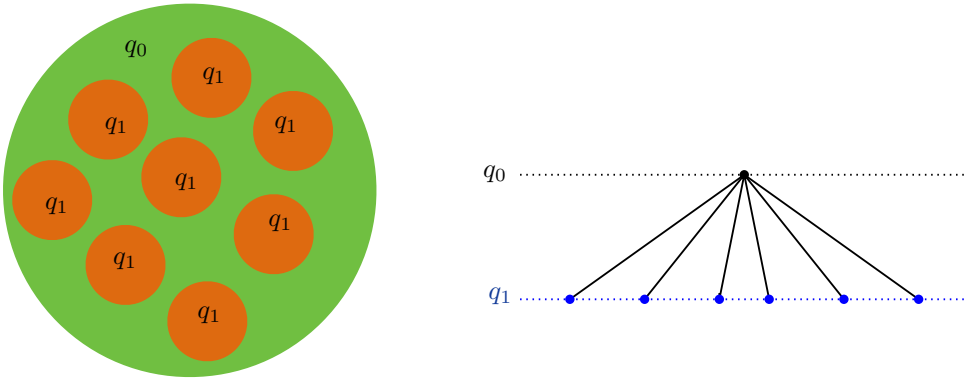


FIG. 14: The 1RSB ultrametric organization of states



### 2. *The probability distribution of the overlap*

Before entering into the fullRSB computation of the phase diagram of the spherical random perceptron we would like to emphasize the physical meaning of the hierarchical ansatz for the overlap matrix. To do this, we consider again the average overlap distribution. For a RS ansatz we have

$$P(q) = \delta(q - q_0) \tag{115}$$

and therefore two typical solutions are at distance $q_0$. We now consider the case in which we assume that the saddle point solution for the overlap matrix is parametrized by a 1RSB ansatz. In this case we have

$$\begin{aligned} P(q) &= \lim_{n\to 0} \frac{1}{n(n-1)} \sum_{a\neq b} \delta(q - Q_{ab}) = \lim_{n\to 0} \frac{1}{n(n-1)} \left[ \frac{n}{m_0} m_0(m_0-1)\delta(q-q_1) + (n^2 - n m_0)\delta(q-q_0) \right] \\ &= (1-m_0)\delta(q-q_1) + m_0\delta(q-q_0)\,. \end{aligned} \tag{116}$$

Since we assume that $q_1 > q_0$ it follows that in this case the solutions of the CSP are organized in *clusters*, see Fig. (14).

If two solutions are in the same cluster, their overlap will be $q_1$, otherwise it will be $q_0$. The average probability distribution that two random solutions are in the same cluster is $1 - m_0$ while it is $m_0$ for two solutions not to

be in the same cluster. Therefore it is meaningful to have $m_0 \in [0,1]$. At this point we can consider the case in which the solution of the saddle point equations for $Q_{ab}$ is of the fullRSB type. Let us compute again

$$P(q) = \lim_{n\to 0} \frac{1}{n(n-1)} \sum_{a\neq b} \delta(q - Q_{ab}) = \lim_{n\to 0} \frac{n}{n(n-1)} \sum_{i=0}^{k} (m_{i-1} - m_i)\delta(q - q_i) \,. \tag{117}$$

In the fullRSB limit, we have that

$$m_{i-1} \simeq m_i - \mathrm{d}x \simeq x - \mathrm{d}x \qquad \{q_i\}_{i=1,\dots,k} \to q(x) \tag{118}$$

and therefore the sum appearing in Eq. (117) becomes

$$P(q) = \lim_{n\to 0} -\frac{1}{n-1} \int_n^1 \mathrm{d}x \delta\left(q - q(x)\right) = \int_0^1 \mathrm{d}x \delta\left(q - q(x)\right) = \left|\frac{\mathrm{d}x(q)}{\mathrm{d}q}\right| \tag{119}$$

being $x(q)$ the inverse function of $q(x)$. Therefore the overlap profile $q(x)$ encodes for the average probability distribution of the overlap.

#### 3. *The ultrametric structure of pure states*

The hierarchical ansatz over the overlap matrix imposes a particular structure for the organization of the solutions of the CSP. In particular it has been discovered in [84] that the solutions are organized in an ultrametric way. We will not discuss here this aspect here but the interested reader can look to [24, 85] for a detailed review.



### E. The fullRSB solution of the spherical random perceptron

We will now turn to the computation of the spherical random perceptron in the region where the RS solution is unstable. In order to perform this computation we will assume that the solution is of the fullRSB type. The plan for the computation will be to analyze separately the entropic and interaction terms of the replicated free energy.

#### 1. *The entropic term*

We want to compute the entropic term given by $\ln\det Q/2$ when $Q$ is a fullRSB matrix parametrized by 1 on the diagonal and $q(x)$ outside. There is a general expression of this term that has been given in [86]. Here we will report only the final formula. The interested reader can look at the Appendix of [86] for a derivation. The entropic term is given by

$$\frac{1}{2} \lim_{n\to 0} \partial_n \ln\det Q = \frac{1}{2}\left[\ln(1 - \langle q\rangle) + \frac{q(0)}{(1-\langle q\rangle)^2} - \int_0^1 \frac{\mathrm{d}x}{x^2} \frac{\lambda(x)}{1 - \langle x\rangle}\right] \tag{120}$$

being

$$\lambda(x) = 1 - xq(x) - \int_x^1 \mathrm{d}y q(y) \qquad \langle q\rangle = \int_0^1 \mathrm{d}y q(y) \,. \tag{121}$$

### 2. The interaction term: Parisi's flow equation

We now turn to the computation of the interaction term. In order to do this, we will follow [87] and the appendix of [75]. The general strategy is to consider a $k$RSB ansatz and then take the $k \to \infty$ limit. Therefore we consider a stepwise profile of $q(x)$ parametrized as if Fig. (13)-left. If we introduce $\mathbf{1}^{(n)}_{m_i}$ as a block diagonal matrix of size $n \times n$ whose diagonal blocks have size $m_i \times m_i$ whose elements are all equal to one, and outside the diagonal blocks are all zeros, then we can write the matrix $Q$ as

$$Q = \sum_{i=0}^{k+1} (q_i - q_{i-1})\, \mathbf{1}^{(n)}_{m_{i-1}} \tag{122}$$

and we are using the convention

$$q_{k+1} = 1 \qquad q_{-1} = 0\,. \tag{123}$$

In this way the interaction term can be written as

$$\mathcal{S}_I = \alpha \ln \exp \left[ \frac{1}{2} \sum_{i=0}^{k+1} (q_i - q_{i-1}) \sum_{l,m=1} \left[ \mathbf{1}^{(n)}_{m_{i-1}} \right]_{lm} \partial_l \partial_m \right] \prod_{s=1}^{n} \theta(h_s) \Big|_{\underline{h}=-\sigma} . \tag{124}$$

Let us now isolate the contribution coming from the innermost block. This is given by

$$\begin{aligned} \mathcal{S}_I &= \alpha \ln \exp \left[ \frac{1}{2} \sum_{i=0}^{k} (q_i - q_{i-1}) \sum_{l,m=1} \left[ \mathbf{1}^{(n)}_{m_{i-1}} \right]_{lm} \partial_l \partial_m \right] \exp \left[ \frac{1}{2} (1 - q_k) \sum_{l=1}^{n} \partial_l^2 \right] \prod_{s=1}^{n} \theta(h_s) \Big|_{\underline{h}=-\sigma} \\ &= \alpha \ln \exp \left[ \frac{1}{2} \sum_{i=0}^{k} (q_i - q_{i-1}) \sum_{l,m=1} \left[ \mathbf{1}^{(n)}_{m_{i-1}} \right]_{lm} \partial_l \partial_m \right] \prod_{s=1}^{n} \gamma_{1-q_k} \star \theta(h_s) \Big|_{\underline{h}=-\sigma} \end{aligned} \tag{125}$$

We now introduce

$$g(1, h) \equiv g(m_k, h) = \gamma_{1-q_k} \star \theta(h) = \Theta \left[ \frac{h}{\sqrt{2(1 - q_k)}} \right] \tag{126}$$

Let us now consider the next innermost sub-block in the differential operator. We get

$$\begin{aligned}
\mathcal{S}_I &= \alpha \ln \exp\left[\frac{1}{2}\sum_{i=0}^{k-1}(q_i - q_{i-1})\sum_{l,m=1}^{n}\left[\mathbf{1}^{(n)}_{m_{i-1}}\right]_{lm}\partial_l\partial_m\right] \\
&\times \exp\left[\frac{1}{2}(q_k - q_{k-1})\sum_{l,m=1}^{n}\left[\mathbf{1}^{(n)}_{m_{k-1}}\right]_{lm}\partial_l\partial_m\right]\prod_{s=1}^{n} g(m_k, h_s)\Big|_{\underline{h}=-\sigma} \\
&= \alpha \ln \exp\left[\frac{1}{2}\sum_{i=0}^{k-1}(q_i - q_{i-1})\sum_{l,m=1}^{n/m_{k-1}}\left[\mathbf{1}^{(n/m_{k-1})}_{m_{i-1}/m_{k-1}}\right]_{lm}\partial_l\partial_m\right] \\
&\times \exp\left[\frac{1}{2}(q_k - q_{k-1})\sum_{l,m=1}^{n/m_{k-1}}\left[\mathbf{1}^{(n/m_{k-1})}_{m_k}\right]_{lm}\partial_l\partial_m\right]\prod_{s=1}^{n/m_{k-1}} g^{m_{k-1}}(m_k, h_s)\Big|_{\underline{h}=-\sigma} \\
&= \alpha \ln \exp\left[\frac{1}{2}\sum_{i=0}^{k-1}(q_i - q_{i-1})\sum_{l,m=1}^{n/m_{k-1}}\left[\mathbf{1}^{(n/m_{k-1})}_{m_{i-1}/m_{k-1}}\right]_{lm}\partial_l\partial_m\right]\prod_{s=1}^{n/m_{k-1}} \gamma_{q_k - q_{k-1}} \star g^{m_{k-1}}(m_k, h_s)\Big|_{\underline{h}=-\sigma} \\
&= \alpha \ln \exp\left[\frac{1}{2}\sum_{i=0}^{k-1}(q_i - q_{i-1})\sum_{l,m=1}^{n/m_{k-1}}\left[\mathbf{1}^{(n/m_{k-1})}_{m_{i-1}/m_{k-1}}\right]_{lm}\partial_l\partial_m\right]\prod_{s=1}^{n/m_{k-1}} g(m_{k-1}, h_s)\Big|_{\underline{h}=-\sigma}
\end{aligned} \tag{127}$$

where we have defined

$$g(m_{k-1}, h) = \gamma_{q_k - q_{k-1}} \star g^{m_{k-1}}(m_k, h)\,. \tag{128}$$

At this point we can go on with the same strategy. Eq. (128) becomes

$$g(m_{i-1}) = \gamma_{q_i - q_{i-1}} \star g^{m_{i-1}/m_i}(m_i, h)\,. \tag{129}$$

Taking the continuum limit we have

$$m_i = x \qquad m_{i-1} \simeq m_i - \mathrm{d}x = x - \mathrm{d}x \qquad q_i - q_{i-1} = \dot{q}(x)\mathrm{d}x \tag{130}$$

and Eq. (129) becomes

$$g(x, h) - \mathrm{d}x\dot{g}(x, h) = g(x, h) + \frac{1}{2}\dot{q}(x)g''(x, h) - \frac{1}{x}g(x, h)\ln g(x, h) \tag{131}$$

and therefore we have

$$\dot{g}(x, h) = -\frac{\dot{q}(x)}{2}g''(x, h) + \frac{1}{x}g(x, h)\ln g(x, h) \tag{132}$$

and we have indicated with primes the derivatives with respect to $h$ and with a dot the derivative with respect to $x$. The partial differential equation (132) has

$$g(1, h) = \gamma_{1-q(1)} \star \theta(h) = \Theta\left[\frac{h}{\sqrt{2(1-q(1))}}\right] \tag{133}$$

as boundary condition. We can now introduce

$$f(x, h) = \frac{1}{x}\ln g(x, h) \tag{134}$$

and the corresponding flow equation is

$$\begin{cases} \dot{f}(x,h) = -\frac{\dot{q}(x)}{2}\left[f''(x,h) + x\left(f'(x,h)\right)^2\right] \\ f(1,h) = \ln\gamma_{1-q(1)} \star \theta(h) = \ln\Theta\left[\frac{h}{\sqrt{2(1-q(1))}}\right] . \end{cases} \tag{135}$$

This equation was derived for the first time by Parisi in the context of the Sherrington-Kirkpatrick model [73]. Note that the particular form of the flow equation is due to the form of the differential operator and therefore it is quite generic. Instead the initial condition strongly depends on the details of the model. At this point we can easily conclude the computation of the interaction term. Indeed at the end of the iterations one gets

$$\mathcal{S}_I = \alpha \ln e^{\frac{q(0)}{2}\partial_h^2} g^{n/m_0}(m_0,h)\Big|_{h=-\sigma} \to n\alpha\gamma_{q(0)} \star f(0,-\sigma) \qquad n \to 0 . \tag{136}$$

### 3. $\mathcal{S}(Q)$ *at the fullRSB level*

Putting together all the pieces we get

$$\lim_{n\to 0}\partial_n \mathcal{S}(Q) = \frac{1}{2}\left[\ln(1-\langle q\rangle) + \frac{q(0)}{(1-\langle q\rangle)^2} - \int_0^1 \frac{\mathrm{d}x}{x^2}\frac{\lambda(x)}{1-\langle x\rangle}\right] + \alpha\gamma_{q(0)} \star f(0,-\sigma) . \tag{137}$$

This expression depends both explicitly and implicitly on $q(x)$. Indeed the function $f(0,-\sigma)$ is the solution of the flow equation (135).

### 4. *The saddle point equations*

At this point we would like to take the saddle point equations of $\mathcal{S}(Q)$ w.r.t. the overlap profile $q(x)$. This is in principle a difficult problem since $\mathcal{S}(Q)$ depends on $q(x)$ also implicitly. A possible solution is to add Lagrange multipliers in order to enforce the flow equation and its boundary condition of Eq. (135) [88]. We call $P(1,h)$ the Lagrange multiplier to enforce the latter while $P(x,h)$ the one to enforce the former. In this way we can write

$$\begin{aligned} \mathcal{S}(Q) = &\frac{1}{2}\left[\ln(1-\langle q\rangle) + \frac{q(0)}{(1-\langle q\rangle)^2} - \int_0^1 \frac{\mathrm{d}x}{x^2}\frac{\lambda(x)}{1-\langle x\rangle}\right] + \alpha\gamma_{q(0)} \star f(0,-\sigma) \\ &- \alpha\int_{-\infty}^{\infty}\mathrm{d}h P(1,h)\left[f(1,h) - \ln\Theta\left[\frac{h}{\sqrt{2(1-q(1))}}\right]\right] \\ &+ \alpha\int_0^1 \mathrm{d}x\int_{-\infty}^{\infty}\mathrm{d}h P(x,h)\left[\dot{f}(x,h) + \frac{\dot{q}(x)}{2}\left[f''(x,h) + x\left(f'(x,h)\right)^2\right]\right] \end{aligned} \tag{138}$$

and the variational equations can be obtained very easily. Indeed taking the functional derivatives with respect to the Lagrange multipliers we get back Eq. (135). Instad taking the functional derivatives w.r.t. $f(x,h)$ and $f(0,h)$ respectively we get

$$\begin{cases} \dot{P}(x,h) = \frac{\dot{q}(x)}{2}\left[P''(x,h) - 2x\left(f'(x,h)P(x,h)\right)'\right] \\ P(0,h) = \frac{1}{\sqrt{2\pi q(0)}}e^{-(h+\sigma)^2/(2q(0))} . \end{cases} \tag{139}$$

Finally we can take the functional derivative with respect to $q(0)$ (and we assume $x \neq 0$[9]). We get

$$0 = \frac{1}{2}\left[\frac{q(0)}{(1-\langle q\rangle)^2} + \int_0^x \mathrm{d}y \frac{\dot{q}(y)}{\lambda^2(y)}\right] + \alpha \frac{\delta}{\delta q(x)} \int_{-\infty}^{\infty} \mathrm{d}h \int_0^1 \mathrm{d}y \dot{q}(y) P(y,h) \frac{1}{2}\left[f''(y,h) + y\left(f'(y,h)\right)^2\right] \tag{140}$$

and integrating by parts the last term we get

$$\begin{aligned} &\frac{\delta}{\delta q(x)} \int_{-\infty}^{\infty} \mathrm{d}h \int_0^1 \mathrm{d}y \dot{q}(y) P(y,h) \frac{1}{2}\left[f''(y,h) + y\left(f'(y,h)\right)^2\right] \\ &= -\int_{-\infty}^{\infty} \mathrm{d}h \frac{\mathrm{d}}{\mathrm{d}x} P(x,h) \frac{1}{2}\left[f''(x,h) + x\left(f'(x,h)\right)^2\right] \end{aligned} \tag{141}$$

and using the flow equations for $P$ and $f$ we get

$$\begin{aligned} &-\frac{1}{2}\int_{-\infty}^{\infty} \mathrm{d}h \frac{\mathrm{d}}{\mathrm{d}x} P(x,h)\left[f''(x,h) + x\left(f'(x,h)\right)^2\right] \\ &= -\frac{1}{2}\int_{-\infty}^{\infty} \mathrm{d}h P(x,h)\left[\frac{\dot{q}(x)}{2}\left(\partial_h^2 + 2x f'(x,h)\partial_h\right) + \frac{\mathrm{d}}{\mathrm{d}x}\right]\left[f''(x,h) + x\left(f'(x,h)\right)^2\right] \\ &= -\frac{1}{2}\int_{-\infty}^{\infty} \mathrm{d}h P(x,h)\left(f'(x,h)\right)^2 \end{aligned} \tag{142}$$

Therefore the final equation of motion is

$$\frac{q(0)}{(1-\langle q\rangle)^2} + \int_0^x \mathrm{d}y \frac{\dot{q}(y)}{\lambda^2(y)} = \alpha \int_{-\infty}^{\infty} \mathrm{d}h P(x,h)\left(f'(x,h)\right)^2 \ . \tag{143}$$

It is quite simple to show that if we plug a replica symmetric profile where $q(x) = q_0$ we get back the replica symmetric saddle point equation (70). Indeed in this case both $P$ and $f$ do not evolve and are equal to their boundary conditions.



### 5. *Marginal stability*

A consequence of the fullRSB equations is *marginal stability*. In order to show it we consider again Eq. (143); since it is valid for all $x \in [0,1]$ we can take the derivative w.r.t. $x$ of both right and left hand side to get

$$\frac{1}{\lambda^2(x)}\dot{q}(x) = \dot{q}(x)\alpha \int_{-\infty}^{\infty} \mathrm{d}h P(x,h)\left(f''(x,h)\right)^2 \tag{144}$$

If $\dot{q}(x) > 0$ then this equation reduces to

$$\frac{1}{\lambda^2(x)} = \alpha \int_{-\infty}^{\infty} \mathrm{d}h P(x,h)\left(f''(x,h)\right)^2 \tag{145}$$

To understand the physical meaning of this relation we compute it on a replica symmetric solution. Note that this is in principle forbidden due to the fact that for a replica symmetric solution $\dot{q} = 0$. However we get

$$\frac{1}{(1-q)^2} = \alpha \int_{-\infty}^{\infty} \frac{\mathrm{d}h}{\sqrt{2\pi q}} e^{-(h+\sigma)^2/(2q)} \left(\frac{\partial^2}{\partial h^2} \ln \Theta\left[\frac{h}{\sqrt{2(1-q)}}\right]\right)^2 \ . \tag{146}$$

---

[9] The equation for $x = 0$ can be obtained from the limit $x \to 0$ [88].

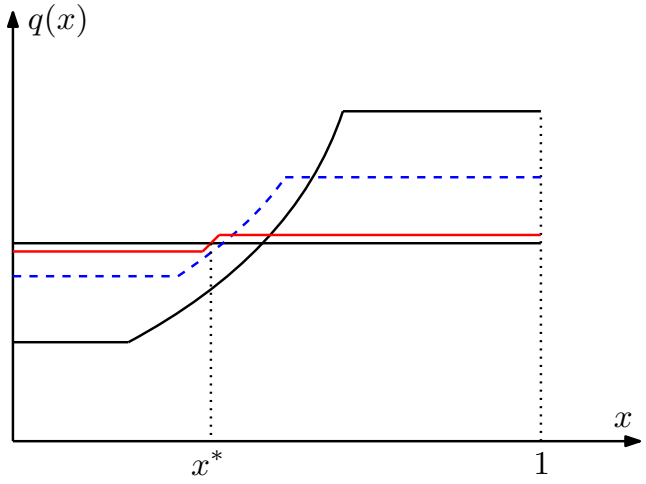


FIG. 15: The scketch of the evolution of $q(x)$ approaching the replica symmetry breaking transition from the broken phase.

This equation is satisfied on the replica symmetric solution exactly at the replica symmetry breaking transition point due to Eq. (111). Why this is so? Let us consider a point in the phase diagram that is in the replica symmetry broken region. Then we try to track the evolution of the overlap profile $q(x)$ when we move from this point towards the replica symmetry breaking transition point. In this way, approaching the de Almeida-Thouless line from the broken phase we have that $q(x)$ evolves as represented in Fig. (15). Therefore one typically has an interval for $x$ where Eq. (145) is satisfied. Of course one can expect that both $P$ and $f$ evolve smoothly when approaching the RSB transition and therefore they converge to their RS expression. This means that exactly at $x = x^*$, represented in Fig. (15) Eq. (145) holds.

Therefore if one has the fullRSB equations, it is quite easy to get where the replica symmetric solution is stable. On top of that, Eq. (145) has a deep physical meaning. One can show that it implies that the fullRSB solution is marginally stable. As we did for the replica symmetric saddle point, we can compute the stability operator coming from a fullRSB solution. This has been done in the context of the Sherrington-Kirkpatrick model close to the replica symmetry breaking transition line [77] and deep in the broken phase [89–92] .

Following this line of reasoning we can compute the derivative w.r.t. $x$ of Eq. (145). We get

$$x\dot{q}(x) = \dot{q}(x)\frac{\lambda(x)}{2}\frac{\int_{-\infty}^{\infty} \mathrm{d}h P(x,h)\left(f'''(x,h)\right)^2}{\int_{-\infty}^{\infty} \mathrm{d}h P(x,h)\left(f''(x,h)\right)^2\left(1+\lambda(x)f'(x,h)\right)} \tag{147}$$

Again, if $x$ is in an interval where $\dot{q}(x) > 0$ we can reduce this equation to

$$x = \frac{\lambda(x)}{2}\frac{\int_{-\infty}^{\infty} \mathrm{d}h P(x,h)\left(f'''(x,h)\right)^2}{\int_{-\infty}^{\infty} \mathrm{d}h P(x,h)\left(f''(x,h)\right)^2\left(1+\lambda(x)f'(x,h)\right)} \,. \tag{148}$$

Following the evolution of this equation coming from the RSB phase to the RS one, we get that on the replica symmetry breaking transition line the *breaking point* of $q(x)$ is given by

$$x^* = \frac{1-q}{2}\frac{\int_{-\infty}^{\infty}\frac{\mathrm{d}h}{\sqrt{2\pi q}}e^{-(h+\sigma)^2/(2q)}\left[\frac{\partial^3}{\partial h^3}\ln\Theta\left[\frac{h}{\sqrt{2(1-q)}}\right]\right]^2}{\int_{-\infty}^{\infty}\frac{\mathrm{d}h}{\sqrt{2\pi q}}e^{-(h+\sigma)^2/(2q)}\left[\frac{\partial^2}{\partial h^2}\ln\Theta\left[\frac{h}{\sqrt{2(1-q)}}\right]\right]^2\left[\frac{1+(1-q)\partial^2}{\partial h^2}\ln\Theta\left[\frac{h}{\sqrt{2(1-q)}}\right]\right]} \tag{149}$$

We will see that Eq. (148) is crucial to study the critical behavior at the jamming transition.

### 6. *The final phase diagram*

We want to close this section by review the phase diagram that can be deduced from the fullRSB equations. Here we will not derive it but the interested reader can look at [46] for the detailed computation. The phase diagram is sketched in Fig. (16).

The red lines separate the replica symmetric phase from the region where replica symmetry is broken. Clearly we see that for $\sigma > 0$ replica symmetry is unbroken, while for $\sigma < 0$ the jamming transition line obtained from the replica symmetry breaking solution is wrong. Therefore the jamming transition in the non-convex regime is described by a fullRSB solution.

For $\sigma < 0$ there are additional phase transition lines. Indeed for $\sigma < \sigma_{\rm 1RSB}$ the replica symmetry breaking transition is towards a 1RSB stable phase and only when the blue line is crossed the 1RSB solution evolves towards a fullRSB one. The blue line is also called the Gardner transition.

For $\sigma < \sigma_{\rm RFOT}$ something new happens. Indeed one realizes that the zero temperature partition function is dominated by solutions with non-zero complexity $\Sigma(s)$. These solutions belong to stable (in the RSB sense) clusters with finite complexity and finite internal entropy $s$. Therefore here the space of solution looks really like what we discuss in the case of coloring and hard spheres. The green line corresponds to the dynamical transition while the dark red line corresponds to the condensation transition where the zero temperature Boltzmann measure is dominated by a sub-exponential number of clusters. Increasing the fraction of constraints $\alpha$ the stable 1RSB ground states undergo a Gardner transition where they split into a fullRSB structure of states. This transition is therefore analogous to what happens in hard spheres upon compression.



## IV. THE JAMMING TRANSITION

In this section we investigate the behavior of the fullRSB equations close to the SAT/UNSAT transition. What we will show is that these equations develops a scaling regime characterized by a set of critical exponents that we will compute. In order to do that it is useful to rewrite the saddle point fullRSB equations in terms of the inverse function of $q(x)$ namely $x(q)$. We will suppose that $q \in [q_m, q_{EA}]$ and correspondingly $x \in [x_m; x_M]$. The saddle point equations are

$$\begin{cases} \dot{f}(q,h) = -\frac{1}{2}\left[f''(q,h) + x(q)\left(f'(q,h)\right)^2\right] \\ f(q_{EA},h) = \ln \gamma_{1-q_{EA}} \star \theta(h) = \ln \Theta\left[\frac{h}{\sqrt{2(1-q_{EA})}}\right] \end{cases}$$
$$\begin{cases} \dot{P}(q,h) = \frac{1}{2}\left[P''(q,h) - 2x\left(f'(q,h)P(q,h)\right)'\right] \\ P(q_m,h) = \frac{1}{\sqrt{2\pi q_m}} e^{-(h+\sigma)^2/(2q_m)} \end{cases} \tag{150}$$
$$\frac{q_m}{(1-\langle q\rangle)^2} + \int_{q_m}^{q} \frac{\mathrm{d}p}{\lambda^2(p)} = \alpha \int_{-\infty}^{\infty} \mathrm{d}h P(q,h)\left(f'(q,h)\right)^2$$
$$\lambda(q) = 1 - q_{EA} + \int_{q}^{q_{EA}} \mathrm{d}p\, x(p)$$

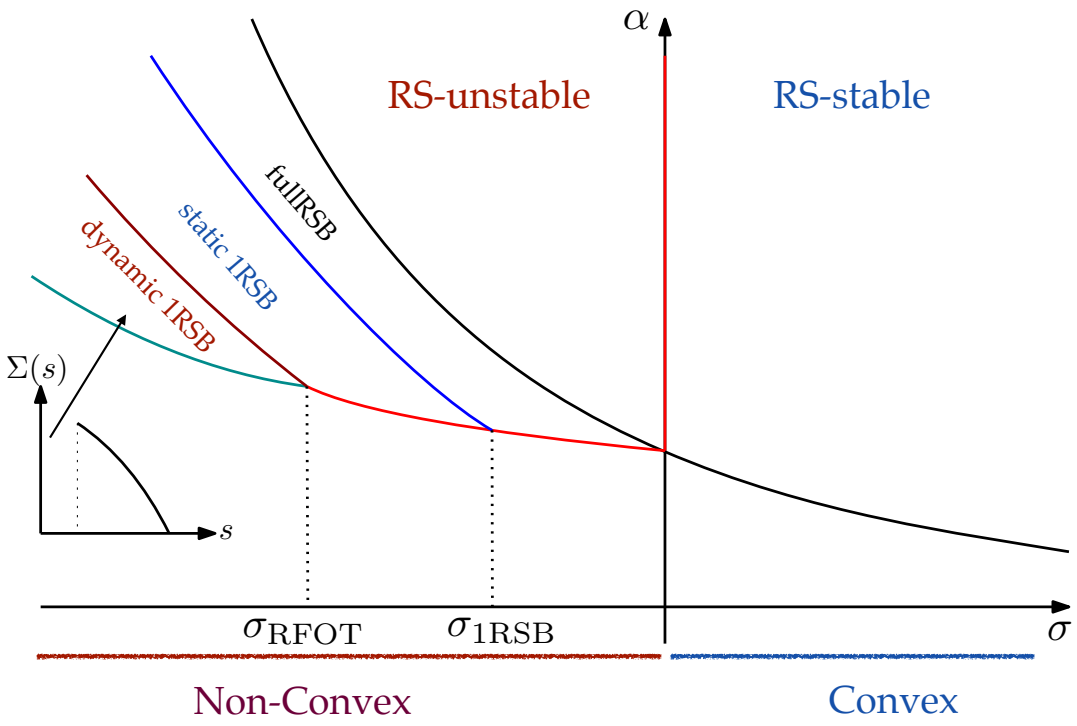


FIG. 16: The phase diagram of the spherical random perceptron. This is a sketch of the phase diagram obtained in [46].

Finally marginal stability implies that

$$\begin{aligned} \frac{1}{\lambda^2(q)} &= \alpha \int_{-\infty}^{\infty} \mathrm{d}h P(q,h) \left(f''(q,h)\right)^2 \\ x(q) &= \frac{\lambda(q)}{2} \frac{\int_{-\infty}^{\infty} \mathrm{d}h P(q,h) \left(f'''(q,h)\right)^2}{\int_{-\infty}^{\infty} \mathrm{d}h P(q,h) \left(f''(q,h)\right)^2 \left(1+\lambda(q) f'(q,h)\right)} \,. \end{aligned} \tag{151}$$

The jamming limit is reached when $q_{EA} \to 1$ which means that the size of the innermost clusters of states goes to zero. Therefore we need to understand how these equations behave when $q_{EA} \to 1$.

We introduce a parameter $\varepsilon$ that denotes the distance form the jamming line: it could be $|\sigma - \sigma_J|$ if the transition is approached when $\alpha$ is kept fixed or $|\alpha - \alpha_J|$ in the opposite case.

We assume that when approaching jamming we have

$$q_{EA} = 1 - \varepsilon^{\kappa} \tag{152}$$

and $\kappa$ is a critical exponent that we will compute. We then define a set of scaling variables and functions:

$$\begin{aligned} y(q) &= \frac{x(q)}{\varepsilon} \\ \hat{f}(q,h) &= \varepsilon f(q,h) \\ \hat{\lambda}(q) &= \frac{\lambda(q)}{\varepsilon} \end{aligned} \tag{153}$$

In this way $y(q) \in [0, 1/\varepsilon]$ and $q \in [q_m, q_{EA}] \to [q_m, 1]$. The scaling solution will emerge in the regime where $q \to 1$. Using Eq. (152) we can also write that for $q \to 1$ we have

$$y(q) \simeq \overline{y}(1-q)^{-1/\kappa} . \tag{154}$$

and $\overline{y}$ is a constant.

Before entering into the description of the scaling equations we want to discuss the physical meaning of Eq. (152) through a parralel in what happens in Hard Spheres.

First we would like to underline again that $q_{EA}$ is the innermost overlap and therefore it is the typical overlap between two solutions that belong to the same innermost cluster.

In the case of Hard Spheres, as we discussed in the first section, the order parameter is the mean square displacement $\Delta_{ab}$ between different configurations. When solved in the high dimensional limit [27], this order parameter becomes a Parisi function $\Delta(x)$ and therefore we denote $\Delta(1) = \Delta_{EA}$. If we monitor the time evolution of the MSD in the glass phase the long time limit is given by Eq. (5). What dynamics is doing is to sample the space of solutions of the packing problem and therefore starting from a solution it will sample solutions that belong to the same cluster. Therefore the plateau of the MSD that is given by $\Delta_{EA}$ has the same physical meaning of $q_{EA}$. When approaching jamming $\Delta_{EA}$ shrinks to zero due to the fact that the compression reduces the space available for the vibrations of the spheres. Therefore one expects $\Delta_{EA} \sim p^{-\kappa}$ being $p$ the pressure. It turns out that the exponent $\kappa$ here has not only the same physical meaning of the one appearing in Eq. (152) but it takes also the same numerical value due to the emerge of *universality*.



### A. Scaling equations close to the jamming line

In order to derive the scaling equations in the jamming limit we start from the flow equation for $f(q,h)$ and then turn to the analysis of the equation for $P(q,h)$. The analysis will closely follow [27, 45, 46].

#### 1. *The flow equation for $f(q,h)$*

The boundary condition for the Parisi equation for $f(q,h)$ is given by

$$f(q_{EA},h) = \ln \gamma_{1-q_{EA}} \star \theta(h) = \ln \Theta\left[\frac{h}{\sqrt{2(1-q_{EA})}}\right] = \begin{cases} 0 & h \to \infty \\ -\frac{h^2}{2(1-q_{EA})} & h \to -\infty \end{cases} \tag{155}$$

We first show that the first equation of (150) has an asymptotic solution of the following form

$$f(q,h) = \begin{cases} 0 & h \to \infty \\ -\frac{h^2}{2\lambda(q)} & h \to -\infty . \end{cases} \tag{156}$$

This ansatz is compatible with Eq. (155). Moreover, the $h \to \infty$ limit is a trivial solution for the flow equation for $f$. Instead for $h \to -\infty$ we have

$$\dot{f}(q,h) \simeq -\frac{x(q)}{2\lambda^2(q)} h^2 \tag{157}$$

while

$$-\frac{1}{2}\left[f''(q,h) + x\left(f'(q,h)\right)^2\right] = -\frac{1}{2}\left[-\frac{1}{\alpha(q)} x(q) \frac{h^2}{\lambda^2(q)}\right] \simeq -\frac{x(q)}{2\lambda^2(q)} h^2 \qquad h \to -\infty \tag{158}$$

and therefore for $h \to -\infty$ the flow equation for $f$ solved by Eq. (156). We now define

$$m(q,h) = \lambda(q) f'(q,h) \tag{159}$$

that satisfies the flow equation

$$\dot{m}(q,h) = -\frac{1}{2} m''(q,h) - \frac{y(q)}{\hat{\lambda}(q)} m(q,h) \left[1 + m'(q,h)\right] . \tag{160}$$

Using Eq. (156) the boundary conditions for this equation are given by

$$m(q,h) = \begin{cases} -h & h \to -\infty \\ 0 & h \to \infty \end{cases} \tag{161}$$

Next we analyze the ratio $y(q)/\hat{\lambda}(q)$ in the jamming limit of $q \to 1$. We have

$$\frac{\upsilon(q)}{\lambda(q)} = \frac{\lambda(q)}{\varepsilon} = \varepsilon^{\kappa-1} + \int_q^{q_{EA}} \mathrm{d}p\, y(p) \simeq \frac{\overline{y}(1-q)^{-1/\kappa}}{\varepsilon^{\kappa-1}\left(1 - \overline{y}\frac{\kappa}{\kappa-1}\right) + \overline{y}\frac{\kappa}{\kappa-1}(1-q)^{(\kappa-1)/\kappa}} \tag{162}$$

and therefore in the scaling region where $1 - q \gg \varepsilon^{\kappa}$ we have

$$\frac{y(q)}{\hat{\lambda}(q)} \simeq \frac{k-1}{k} \frac{1}{1-q} . \tag{163}$$

At this point we consider the following scaling ansatz for $m(q,h)$ in the limit $q \to 1$

$$m(q,h) = -\sqrt{1-q}\, \mathcal{M}\left(\frac{h}{\sqrt{1-q}}\right) \qquad \mathcal{M}(t \to \infty) = 0 \qquad \mathcal{M}(t \to -\infty) \simeq t \tag{164}$$

Plugging this ansatz in Eq. (160) and using Eq. (163) we get

$$\mathcal{M}(t) - t\mathcal{M}'(t) = \mathcal{M}''(t) + 2\frac{\kappa-1}{\kappa} \mathcal{M}(t)\left(1 - \mathcal{M}'(t)\right) \tag{165}$$

Therefore, having fixed $\kappa$, this equation admits a unique solution for the scaling function $\mathcal{M}(t)$ satisfying the boundary conditions of Eq. (164).

### 2. *The flow equation for $P(q,h)$*

We now turn to the study of the flow equation for $P(q,h)$. In this case the boundary condition is

$$P(q_m, h) = \gamma_{q_m}(h + \sigma) . \tag{166}$$

As we have done in the case of $f(q,h)$ we want to consider the limiting behavior for $h \to \pm\infty$. For $h \to \infty$ we can use the fact that $f(q,h) \to 0$ and we have

$$\dot{P}(q,h) \simeq -\frac{1}{2} P''(q,h) \tag{167}$$

which is solved by

$$P(q,h)\gamma_q(h+\sigma) \qquad h \to \infty . \tag{168}$$

For $h \to -\infty$ the flow equation becomes

$$\dot{P}(q,h) = \frac{1}{2}\left[P''(q,h) + 2\frac{y(q)}{\hat{\lambda}(q)}\left(P'(q,h)h + P(q,h)\right)\right] \tag{169}$$

and we have used $f(q,h) \simeq -h^2/(2\lambda(q))$. Using again Eq. (163) we can show that

$$P(q,h) \sim \sqrt{D(q)}e^{-D(q)h^2} \tag{170}$$

is a solution of Eq. (169) if $D(q)$ satisfies the following equation

$$\dot{D}(q) = -2D^2(q) + 2D(q)\frac{\kappa-1}{\kappa}\frac{1}{1-q}\,. \tag{171}$$

If $\kappa < 2$ (as we will see) we get that

$$D(q) = \overline{D}(1-q)^{-2(\kappa-1)/\kappa} \tag{172}$$

Thus for $q \to 1$ we get that

$$P(q,h) = \begin{cases} (1-q)^{(1-\kappa)/\kappa}P_-(h(1-q)^{(1-\kappa)/\kappa}) & h \sim -(1-q)^{-(1-\kappa)/\kappa} \\ P_+(h) & h \gg \sqrt{1-q} \end{cases} \tag{173}$$

Therefore there should be a matching scaling regime that links the scaling function $P_-$ to $P_+$. We therefore conjecture that the scaling solution for $P$ when $q \to 1$ is

$$P(q,h) = \begin{cases} (1-q)^{(1-\kappa)/\kappa}P_-(h(1-q)^{(1-\kappa)/\kappa}) & h \sim -(1-q)^{-(1-\kappa)/\kappa} \\ (1-q)^{-a/\kappa}P_0(h(1-q)^{-1/2}) & |h| \sim \sqrt{1-q} \\ P_+(h) & h \gg \sqrt{1-q} \end{cases} \tag{174}$$

where $a$ is a scaling exponent. The scaling regime in between has as scaling variable $t = h/\sqrt{1-q}$ that coincides with the scaling variable entering in Eq. (165). Indeed this choice gives a non-trivial scaling equation for $P_0$.

The three scaling regime should match and therefore the three scaling functions $P_-$, $P_0$ and $P_+$ should match. For $h < 0$ if we suppose that

$$\begin{array}{ll} P_-(t) \sim |t|^\theta & t \to 0^- \\ P_0^(t) \sim |t|^\theta & t \to -\infty \end{array} \tag{175}$$

we get that $\theta = (2(1-\kappa+a))/(\kappa-2)$ . Instead for $h > 0$ we assume that

$$\begin{array}{ll} P_0^(t) \sim t^{-\gamma} & t \to \infty \\ P_+(t) \sim t^{-\gamma} & t \to 0^+ \end{array} \tag{176}$$

and we obtain that $\gamma = 2a/\kappa$. Plugging the scaling ansatz of Eq. (174) inside the flow equation we get a scaling equation for $P_0$ given by

$$\begin{array}{l} \frac{a}{\kappa}P_0(t) + \frac{1}{2}tP_0(t) = \frac{1}{2}P_0''(t) + \frac{k-1}{k}\left(P_0(t)\mathcal{M}(t)\right)' \\ P_0(t \to -\infty) \sim |t|^{(2(1-\kappa+a))/(\kappa-2)} \qquad P_0(t \to \infty) \sim t^{-2a/\kappa} \end{array} \tag{177}$$

Having fixed $\kappa$, and having computed $\mathcal{M}(t)$ as the solution of the scaling equation (165), Eq. (177) admits only one solution for $P_0(t)$ satisfying both boundary condition at a unique value of $a = a(\kappa)$.

### 3. Fixing the exponent $\kappa$

The exponent $\kappa$ can be fixed finally by Eq. (151). Indeed for $q \to 1$ it becomes

$$\frac{\kappa - 1}{\kappa} = \frac{1}{2} \frac{\int_{-\infty}^{\infty} \mathrm{d}t P_0(t) \left(\mathcal{M}''(t)\right)^2}{\int_{-\infty}^{\infty} \mathrm{d}t P_0(t) \left(\mathcal{M}'(t)\right)^2 \left(1 + \mathcal{M}'(t)\right)} \,. \tag{178}$$

The numerical solution of these equations gives $\kappa = 1.4157\ldots$. The corresponding value of $a$ is $a = 0.2921\ldots$.

## B. Critical exponents of the jamming transition: universality

We have already discussed the physical meaning of the exponent $\kappa$. The exponent $\gamma$ is connected with the distribution of gaps at jamming. Having a solution of the CSP at jamming, one can look at the distribution of positive gaps $h_\mu > 0$. It can be shown that [27, 46]

$$g(h) \sim h^{-\gamma} \qquad h \to 0^+ \,. \tag{179}$$

Furthermore the exponent $\theta$ is connected to the behavior of the distribution of *forces* at jamming. Indeed one can think about approaching the jamming transition form the jammed phase. In this case there is a finite fraction of negative gaps $h_\mu < 0$. Negative gaps are also called forces because in the context of jammed packings of harmonic soft spheres they represent the forces between overlapping spheres. It turns out that the distribution of forces behaves as

$$P(f) \sim f^{\theta} \qquad f \to 0^+ \,. \tag{180}$$

Finally one can show that in the scaling limit the first equation of (151) imply that at jamming the packings are isostatic and therefore the isostaticity index $c$ is equal to 1. All this phenomenology is analogous to the jamming behavior of hard sphere packings and the scaling equations arising for the perceptron that fix the scaling exponents are the same as the ones arising for hard spheres in infinite dimension. Therefore the two problems are in the same universality class.



### 1. Back to Hard Spheres: scaling relation between critical exponents

It turns out that within the numerical precision

$$a = 1 - \frac{\kappa}{2} \tag{181}$$

which is therefore a scaling relation between the two critical exponents. When expressed in terms of the physical critical exponents, this implies

$$\gamma = \frac{1}{2 + \theta} \,. \tag{182}$$

This scaling relation has been derived firstly in the context of hard spheres by M. Wyart in [14, 16]. The same argument to obtain it can be translated in the context of the perceptron [45]. However here we will reproduce the original one for hard spheres.

The way to obtain Eq. (182) is a stability argument. *Mutatis mutandis* it is an argument in the same spirit as the same argument which gives a linear pseudogap in the distribution of frozen fields at zero temperature in the Sherrington-Kirkpatrick model [16, 93].

Let us consider a jammed packing of hard spheres. We assume the packing to be isostatic and therefore mechanically stable. Let us consider what happens when a dipolar force $F$ is applied to two spheres in contact. If the dipolar force is equal to the force that the two spheres are doing one onto the other, the two spheres will separate by a given amount $l$ and the system will collectively flow along a *floppy mode*. A floppy mode is a collective displacement of the spheres in which all spheres in contact (apart the two affected by the dipolar force) stay in contact and therefore they just slide one onto the other. In this way we have

$$p\Delta V \simeq Fl - CNl^2 \tag{183}$$

where $p$ is the (constant) pressure, $\Delta V$ is the variation of the volume induced by the flow of the system and $C$ is a constant. $N$ is the system size. If $l > l^* = F/(CN)$ the system flows towards a more compact configuration. The smallest $l^*$ is obtained considering the contacts that carry the smallest forces. The smallest force can be estimated assuming that the distribution of contact forces is given by Eq. (180) and it is of the order of $F_{\min} \sim N^{1/(1+\theta)}$. Therefore the minimal gap beyond which the packing is destabilized is $l^*_{\min} \sim N^{-\theta/(1+\theta)}$. However when the system is flowing along the floppy mode and the gap $l$ is opening between the two spheres, it could be that a new contact is formed somewhere in the system thus restoring isostaticity and blocking the flow. In order to estimate when this happens, one can assume that the typical $l$ at which a new contact is formed is of the order of the minimal gap between non-touching spheres. This can be estimated by assuming Eq. (179) and is given by $h_{\min} \sim N^{-1/(1+\gamma)}$. The stability of the packing requires that $l^*_{\min} \geq h_{\min}$ which gives $\gamma \geq 1/(2+\theta)$.

In the last years, an extensive amount of numerical simulations on the critical properties of jammed packings of hard spheres in finite dimension has been performed. It turns out that the critical exponents of the jamming transition are extremely robust and do not display any apparent dimensional dependence[10] and the infinite dimensional solution of the hard sphere model (whose critical exponents coincide with the ones of the perceptron) seem to agree with the numerical simulations in three dimensions. The reason why mean field theory gives so good and nontrivial predictions in three dimensions is currently under investigation and it is an open problem in the field. Finally, numerically it is found that the stability bound between the exponent $\gamma$ and $\theta$ that was derived in [14] is saturated. This means that amorphous packings are on the verge of being destabilized and therefore are said to be marginally stable. It is very interesting to note that these properties, both the scaling relations and the isostaticity of jammed packings, is deeply related to the marginal stability of the fullRSB solution and to replica symmetry breaking.



## V. THE TAP APPROACH TO THE SPHERICAL RANDOM PERCEPTRON

In this section we discuss the Thouless-Anderson-Palmer (TAP) approach to the random spherical perceptron. The plan of this section will be to derive the TAP equations from the Belief Propagation (BP) equations and show that the replica symmetric result can be recovered.

The TAP approach for the perceptron was first developed by M. Mézard in [51, 95] using the *cavity method* and in [96] for the case of spherical variables using a large $N$ expansion. Here we will not reproduce these computations but we will closely follow an alternative way that has been reviewed in [97].

---

[10] This statement is not completely true. The exponent that characterize the small force behavior is indeed dimensional dependent but because of simple geometric reasons. Indeed it is dominated by *bucklers*, spheres with $d+1$ contacts whose density vanishes in the high dimensional limit. Once these spheres are removed from the statistical analysis of contact forces, one recovers the mean field critical exponent [94].

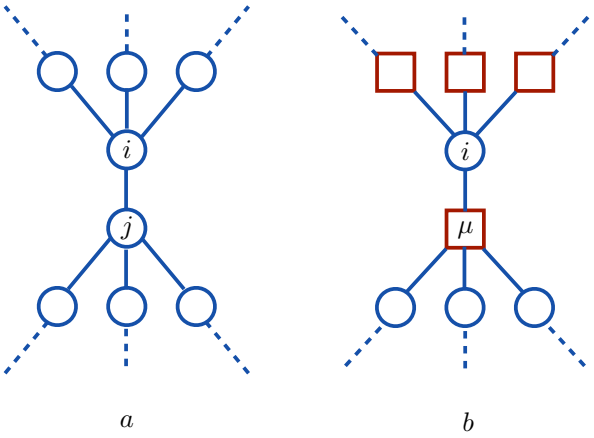


FIG. 17: *a)* The factor graph for a model with pairwise interaction with the topology of a tree. *b)* The same as *a)* but with multispin interaction.



In order to do that we will first derive the belief propagation equations and then we will apply them to the spherical random perceptron.

### A. The belief propagation equations

Let us consider a statistical mechanics model defined with a set of variables $\{x_i\}_{i=1,\dots,N}$ and whose topology is a tree as in Fig. (17.a). By this we mean that the partition function can be written as

$$Z = \int_{\mathbb{R}^N} \mathrm{d}\underline{x} \left[\prod_{i=1}^{N} f_S(x_i)\right] \left[\prod_{i\sim j} f_L(x_i, x_j)\right] . \tag{184}$$

The term $f_S(x_i)$ takes into account for a local field-like term on the variables while the second product runs over $i \sim j$ where $i$ and $j$ are nearest neighbors on the tree.

Let us consider what happens if we remove the link connecting the site $i$ with the site $j$ from the tree. In this case the lattice becomes disconnected. Therefore one can introduce the marginal probability distribution of the variable $x_i$ when the link between $i$ and $j$ is removed. We denote this probability distribution as $m_{i\to j}(x_i)$.

Let us now look at the sub-tree that contains the variable $i$. We can consider the sub-trees obtained by removing the links $i \sim k$ being $k$ a site connected to $i$. In this case we denote the probability distribution $m_{k\to i}(x_k)$ as the marginals of the spins $x_k$ when the links $i \sim k$ are removed. It is very easy to write $m_{i\to j}(x_i)$ as a function of $m_{k\to i}(x_k)$. Indeed we have

$$m_{i\to j}(x_i) = \frac{f_S(x_i)}{z_{i\to j}} \prod_{k\in\partial i\setminus j} \int \mathrm{d}x_k m_{k\to i}(x_k) f_L(x_i, x_k) \tag{185}$$

and the notation $k \in \partial i\setminus j$ runs over all sites $k$ that are connected to $i$ but neglecting $j$. This equation can be explained in the following way:

- $f_S(x_i)$ is the probability (apart from a normalization factor) that if the spin $x_i$ is isolated it is equal to $x_i$.
- $f_L(x_i, x_j)$ is the probability (apart from a normalization factor) that if the spin $k$ is fixed to $x_k$ then the spin $i$ is equal to $x_i$.

Therefore Eq. (185) can be just seen as the composition law for probabilities and therefore $z_{i\to j}$ is just a normalization constant.

Eq. (185) holds for a model in which the interactions are pairwise. As we have seen instead, the perceptron is defined on a bipartite factor graph. Therefore let us consider a model defined on a tree factor graph as in Fig. (17.b). The partition function can be written as

$$Z = \int_{\mathbb{R}^N} \mathrm{d}\underline{x} \left[\prod_{i=1}^{N} f_S(x_i)\right] \left[\prod_{\mu} f_C(\underline{x}_\mu)\right] \tag{186}$$

where $\underline{x}_\mu = \{x_k\}_{k\in\partial\mu}$ is the set of variables that enter in the check (or interaction node) $\mu$. It is quite straightforward to generalize the BP equations to this case. Indeed, defining $m_{i\to\mu}(x_i)$ as the marginal probability distribution of the variable $i$ once the interaction $\mu$ is cut out, we have

$$m_{i\to\mu(x_i)} = \frac{f_S(x_i)}{\tilde{z}_{i\to\mu}} \prod_{\nu\in\partial i\setminus\mu} \int \left[\prod_{j\in\partial\nu\setminus i} \mathrm{d}x_j m_{j\to\nu}(x_j)\right] f_C(\underline{x}_\nu) \tag{187}$$

This equation can be simplified defining

$$\tilde{m}_{\nu\to i}(x_i) = \frac{1}{z_{\nu\to i}} \int \left[\prod_{j\in\partial\nu\setminus i} \mathrm{d}x_j m_{j\to\nu}(x_j)\right] f_C(\underline{x}_\nu) \tag{188}$$

and it becomes

$$m_{i\to\mu(x_i)} = \frac{f_S(x_i)}{z_{i\to\mu}} \prod_{\nu\in\partial i\setminus\mu} m_{\nu\to i}(x_i)\,. \tag{189}$$

The constants $z_{\nu\to i}$ and $z_{i\to\mu}$ are just normalization constant so that the $m$s and $\tilde{m}$s are normalized to one. Eqs. (188) and (189) are thus the belief propagation equations for a bipartite factor graph.

The BP equations are strictly valid on factor graphs that are trees and they can be proven by doing the construction we have done but starting from the leaves of the graph and going through it up to the bulk. However it can be shown that the BP equations can be used also in other two remarkable cases

- *locally tree-like factor graphs in the large size limit*: this is the case of factor graphs with the topology of random regular graphs or Erdös-Renyi graphs described in Sec.1. In this case it can be shown that such random graphs, in the thermodynamic limit are locally tree like being the loops of size $\ln N$. Statistical mechanics model can be analyzed even rigorously on these topologies [98, 99].
- *fully connected models*: these are models where each variable enters in all interaction nodes of the factor graph but its contribution to the interaction term is small and tends to zero with the system size. The random perceptron model we are defining here belongs to this class. Indeed each variable enters in each constraint $\mu$ through a coupling $W_i^\mu \equiv \xi_i^\mu/\sqrt{N}$ which is of order $1/\sqrt{N}$. Therefore in this case, removing one link in the graph as we do in the BP construction is a small perturbation.

Before entering into the application of the BP equations to the case of the spherical random perceptron we want to show how to compute the magnetizations and variances of single variables using this method. Thus let us consider

$$\langle x_i \rangle = \int \mathrm{d}x_i m_i(x_i) \tag{190}$$

where $m_i(x_i)$ is the real marginal of the spin $i$ when no link is removed from the graph. $m_i(x_i)$ can be easily computed using the *cavity* marginals $m_{i\to\mu}$. Indeed we have

$$m_i(x_i) = \frac{f_S(x_i)}{\tilde{z}_i} \prod_{\nu\in\partial i} \int \left[ \prod_{j\in\partial\nu\setminus i} \mathrm{d}x_j m_{j\to\nu}(x_j) \right] f_C(\underline{x}_\nu) \equiv \frac{f_S(x_i)}{z_i} \prod_{\nu\in\partial i} m_{i\to\mu(x_i)} \tag{191}$$

We now write Eqs. (188) and (189) in the case of the spherical perceptron. The partition function is

$$Z_\xi = \int \mathcal{D}\underline{X} \prod_{\mu=1}^{M} e^{-\beta v(h_\mu)} \,. \tag{192}$$

In order to write the BP equations we need to have independent variables $x_i$. Instead in our case the variables are coupled with a global spherical constraint that is contained in the measure $\mathcal{D}X$. In order to avoid this problem we introduce a Lagrange multiplier $\lambda$ so that

$$Z_\xi \propto \int_{\mathbb{R}^N} \mathrm{d}\underline{X} \left[ \prod_{i=1}^{N} e^{-\frac{\lambda}{2}x_i^2} \right] \left[ \prod_{\mu=1}^{M} e^{-\beta v(h_\mu)} \right] \tag{193}$$

and $\lambda$ is fixed a posteriori in order to enforce the spherical constraint. At this point the partition function is the same form as Eq. (186). Therefore we can easily write the BP equations that are

$$\begin{aligned} m_{i\to\mu}(x_i) &\sim e^{-\lambda x_i^2/2} \prod_{\nu(\neq\mu)} \tilde{m}_{\nu\to i}(x_i) \\ \tilde{m}_{\nu\to i}(x_i) &\sim \int \left[ \prod_{k(\neq i)} \mathrm{d}x_k m_{k\to\nu}(x_k) \right] e^{-\beta v(h_\nu)} \qquad h_\nu = \underline{W}^\nu \cdot \underline{X} - \sigma \equiv z_\nu - \sigma \end{aligned} \tag{194}$$

and we have defined $z_\mu = \underline{W}^\mu \cdot \underline{X}$. Note that in writing Eqs. (194) we have explicitly used the fact that the factor graph is fully connected and we have neglected the normalization constants that will not be important for what follows.

### B. Gaussian parametrization of BP marginals and relaxed-BP algorithm

It turns out that fully connected models are characterized only by the local magnetizations and variances of the variables [35]. This is due to the fact that the interactions between the dynamical variables are given in terms of sum of a very large number of terms and therefore the central limit theorem can be applied. Therefore we consider the following ansatz

$$m_{k\to\nu}(x_k) \sim e^{-\frac{(x_k - a_{k\to\nu})^2}{2v_{k\to\nu}}} \,. \tag{195}$$

By definition we have

$$a_{i\to\mu} = \int \mathrm{d}x_i m_{i\to\mu}(x_i) x_i \qquad v_{i\to\mu} = \int \mathrm{d}x_i m_{i\to\mu}(x_i) x_i - a_{i\to\mu}^2 \,. \tag{196}$$

Plugging this ansatz inside the second equation of Eqs. (194) we get

$$\tilde{m}_{\nu\to i}(x_i) \sim e^{-A_{\nu\to i}x_i^2/2 + B_{\nu\to i}x_i} \tag{197}$$

where

$$\begin{aligned} A_{\nu\to i} &= -(W_i^\nu)^2 \partial_\omega \mathcal{R}\left(\omega_{\nu\to i}, V_{\nu\to i}\right) \\ B_{\nu\to i} &= W_i^\nu \mathcal{R}\left(\omega_{\nu\to i}, V_{\nu\to i}\right) \end{aligned} \tag{198}$$

and we have used the shorthand notation $\partial_\omega \mathcal{R}\left(\omega_{\nu\to i}, V_{\nu\to i}\right) \equiv \partial_{\omega_{\nu\to i}} \mathcal{R}\left(\omega_{\nu\to i}, V_{\nu\to i}\right)$. The function $R(\omega, V)$ is defined as

$$\mathcal{R}(\omega, V) = \frac{1}{V} \frac{\int \mathrm{d}z e^{-\beta v(z-\sigma) - \frac{1}{2V}(z-\omega)^2}(z-\omega)}{\int \mathrm{d}z e^{-\beta v(z-\sigma) - \frac{1}{2V}(z-\omega)^2}} \tag{199}$$

Therefore we have

$$\begin{aligned} \prod_{\nu(\neq\mu)} \tilde{m}_{\nu\to i}(x_i) &\sim e^{-\frac{(x_i - T_{i\to\mu})^2}{2\hat{\sigma}_{i\to\mu}}} \\ \hat{\sigma}_{i\to\mu} &= \left[\sum_{\nu(\neq\mu)} A_{\nu\to i}\right]^{-1} \\ T_{i\to\mu} &= \hat{\sigma}_{i\to\mu} \sum_{\nu(\neq\mu)} B_{\nu\to i} \end{aligned} \tag{200}$$

and plugging this inside the first equation of (194) we get

$$m_{i\to\mu}(x_i) \sim e^{-\lambda x_i^2/2} e^{-\frac{(x_i - T_{i\to\mu})^2}{2\hat{\sigma}_{i\to\mu}}} \tag{201}$$

We can use this expression to close the equations. Indeed using Eq. (196) we get

$$\begin{aligned} a_{i\to\mu} &= \int \mathrm{d}x_i \, x_i m_{i\to\mu}(x_i) = f_a(\hat{\sigma}_{i\to\mu}, T_{i\to\mu}) \\ v_{i\to\mu} &= \int \mathrm{d}x_i \, x_i^2 m_{i\to\mu}(x_i) - a_{i\to\mu}^2 = \hat{\sigma}_{i\to\mu} \partial_T f_a(\hat{\sigma}_{i\to\mu}, T_{i\to\mu}) \, . \end{aligned} \tag{202}$$

where the function $f_a(\hat{\sigma}, T)$ is given by

$$f_a(\hat{\sigma}, T) = \frac{\int \mathrm{d}x \, e^{-\lambda x_i^2/2 - \frac{(x-T)^2}{2\hat{\sigma}}} x}{\int \mathrm{d}x \, e^{-\lambda x_i^2/2 - \frac{(x-T)^2}{2\hat{\sigma}}}} = \frac{T}{1+\lambda\hat{\sigma}} \tag{203}$$

Eqs. (198), (200) and (202) can be used as an iterative algorithm that is called *relaxed-BP*[11]. One starts with an initial set of $\{a_{i\to\mu}\}$ and $\{v_{i\to\mu}\}$ and iterates the equations up to convergence. The algorithm always converges to a unique fixed point in the replica symmetric phase and we will not discuss what happens in the RSB phase. Once the algorithm has converged to a fixed point one can evaluate the effective magnetization and variance of each variable using Eq. (191). In this way we have

$$\begin{aligned} a_i &= \langle x_i \rangle = f_a(\hat{\sigma}_i, T_i) \qquad & v_i &= \langle (x_i - \langle x_i \rangle)^2 \rangle = \hat{\sigma}_i \partial_T f_a(\hat{\sigma}_i, T_i) \\ \hat{\sigma}_i &= -\left[\sum_\nu A_{\nu\to i}\right]^{-1} & T_i &= \hat{\sigma}_i \sum_\nu B_{\nu\to i} \, . \end{aligned} \tag{204}$$

[11] The term *relaxed* comes from the fact that we have relaxed the functional dependence of the BP equations to Gaussian functions.

Therefore iterating the relaxed-BP algorithm one has access to magnetizations and variances. It is important to note that these equations hold for a fixed disorder realization. This represents a difference with respect to the replica method which gives the results of the average over different realizations of the $\{\underline{W}^{\mu}\}$.

### C. TAPyification

The relaxed-BP algorithm involves order $N^2$ variables that enter in the iterative equations and which live on the links between variables $x_i$ and check nodes. This algorithm can be further simplified using only order $N$ variables which is extremely important from a computational point of view. In order to do that let us consider

$$\omega_{\mu\to i} = \sum_{k(\neq i)} W_k^{\mu} a_{k\to\mu} = \omega_{\mu} - W_i^{\mu} a_{i\to\mu} \qquad \omega_{\mu} = \sum_{k=1}^{N} W_k^{\mu} a_{k\to\mu} \tag{205}$$

The term $W_i^{\mu} a_{i\to\mu}$ is of order $1/\sqrt{N}$ and therefore is a small perturbation. We will track it through the iterative equations using perturbation theory. We first have that

$$V_{\mu\to i} = \sum_{k(\neq i)} \left(W_i^{\mu}\right)^2 v_{k\to\mu} \simeq V_{\mu} \equiv \sum_{k} \left(W_i^{\mu}\right)^2 v_{k\to\mu} \tag{206}$$

since the correction is of the order of $1/N$.

We next consider Eqs. (198). We get

$$\begin{aligned} A_{\mu\to i} &= -\left(W_i^{\mu}\right)^2 \partial_{\omega}\mathcal{R}(\omega_{\mu\to i}, V_{\mu\to i}) \simeq -\left(W_i^{\mu}\right)^2 \partial_{\omega}\mathcal{R}(\omega_{\mu}, V_{\mu}) \\ B_{\mu\to i} &= W_i^{\mu}\mathcal{R}(\omega_{\mu\to i}, V_{\mu\to i}) \simeq W_i^{\mu}\mathcal{R}(\omega_{\mu}, V_{\mu}) - \left(W_i^{\mu}\right)^2 a_{i\to\mu}\partial_{\omega}\mathcal{R}(\omega_{\mu}, V_{\mu}) \end{aligned} \tag{207}$$

and since

$$\begin{aligned} a_i &= f_a(\hat{\sigma}_i, T_i) \\ v_i &= \hat{\sigma}_i \partial_T f_a(\hat{\sigma}_i, T_i) \end{aligned} \tag{208}$$

we have

$$\begin{aligned} \hat{\sigma}_i &= \sum_{\mu=1}^{M} A_{\mu\to i} \simeq -\left[\sum_{\mu=1}^{M} \left(W_i^{\mu}\right)^2 \mathcal{R}(\omega_{\mu}, V_{\mu})\right]^{-1} \\ \hat{T}_i &= \hat{\sigma}_i \sum_{\mu=1}^{M} B_{\nu\to i} \simeq \sigma_i \left[\sum_{\mu} W_i^{\mu}\mathcal{R}(\omega_{\mu}, V_{\mu}) - \sum_{\mu=1}^{M} a_{i\to\mu}\left(W_i^{\mu}\right)^2 \partial_{\omega}\mathcal{R}(\omega_{\mu}, V_{\mu})\right] . \end{aligned} \tag{209}$$

At this point we take back the equations for $a_{i\to\mu}$ and $v_{i\to\mu}$. We have

$$\begin{aligned} a_{i\to\mu} &= f_a\left(\hat{\sigma}_{i\to\mu}, T_{i\to\mu}\right) \simeq f_a\left(\hat{\sigma}_i, T_i - \hat{\sigma}_i B_{\mu\to i}\right) \simeq f_a(\hat{\sigma}_i, T_i) - \hat{\sigma}_i B_{\mu\to i}\partial_T f_a(\hat{\sigma}_i, T_i) \\ &\simeq a_i - v_i W_i^{\mu}\mathcal{R}(\omega_{\mu}, V_{\mu}) \\ v_{i\to\mu} &\simeq v_i = \hat{\sigma}_i \partial_T f_a(\hat{\sigma}_i, T_i) . \end{aligned} \tag{210}$$

Therefore we have

$$\begin{aligned} \omega_{\mu} &= \sum_{k=1}^{N} W_k^{\mu} a_{k\to\mu} \simeq \sum_{k=1}^{N} W_k^{\mu} a_k - \sum_{k=1}^{N} (W_k^{\mu})^2 v_k \mathcal{R}(\omega_{\mu}, V_{\mu}) = \sum_{k=1}^{N} W_k^{\mu} a_k - V_{\mu}\mathcal{R}(\omega_{\mu}, V_{\mu}) \\ V_{\mu} &= \sum_{k=1}^{N} (W_k^{\mu})^2 v_k . \end{aligned} \tag{211}$$

Eqs. (207), (208), (209) and (211) represent the *generalized*-AMP algorithm[12]. This algorithm can be further simplified. Indeed one has that in the thermodynamic limit $(W_i^\mu)^2 \simeq 1/N$ and therefore $V_\mu = V$ and $\hat{\sigma}_i = \hat{\sigma}$ are constants. We next assume to be in the SAT phase so that

$$\mathcal{R}(\omega, V) = \partial_\omega \ln \Theta \left[ \frac{\omega - \sigma}{\sqrt{2V}} \right] . \tag{212}$$

The new equations are the TAP equations

$$\begin{aligned} &\omega_\mu = \sum_{k=1}^{N} W_k^\mu a_k - V\mathcal{R}(\omega_\mu, V) \qquad T_i = \hat{\sigma} \left[ \sum_{\mu=1}^{M} W_i^\mu \mathcal{R}(\omega_\mu, V) - \frac{a_i}{N} \sum_{\mu=1}^{M} \partial_\omega \mathcal{R}(\omega_\mu, V) \right] \\ &a_i = \frac{T_i}{1 + \lambda\hat{\sigma}} \qquad \hat{\sigma}^{-1} = -\frac{1}{N} \sum_{\mu=1}^{M} \mathcal{R}(\omega_\mu, V) \qquad V = \frac{\hat{\sigma}}{1 + \lambda\hat{\sigma}} \end{aligned} \tag{213}$$

These equations can be implemented as an algorithm to extract local magnetizations[13] and therefore it is very powerful in applications such as machine learning and inference. Eqs. (213) depend on the Lagrange multiplier $\lambda$. This must be fixed by enforcing the spherical constraint and therefore we have

$$V = \frac{1}{N} \sum_{i=1}^{N} v_i = \frac{1}{N} \sum_{i=1}^{N} \left( \langle x_i^2 \rangle - \langle x_i \rangle^2 \right) = 1 - \frac{1}{N} \sum_{i=1}^{N} a_i^2 = 1 - q \tag{214}$$

where we have denoted with $q$ the overlap

$$q = \frac{1}{N} \sum_{i=1}^{N} a_i^2 . \tag{215}$$

### D. Getting back the replica results

Starting from Eqs. (213) we want to recover the results that we have obtained through the replica method. First of all, using that $V = 1 - q$ we have that

$$q_i = \frac{1 - q}{\hat{\sigma}} T_i \tag{216}$$

and therefore

$$q = \frac{1}{N} \sum i = 1^N a_i^2 = \frac{(1-q)^2}{\hat{\sigma}^2} \frac{1}{N} \sum_{i=1}^{N} T_i^2 . \tag{217}$$

Furthermore we have

$$T_i^2 \simeq \hat{\sigma}^2 \left[ \sum_{\mu=1}^{M} W_i^\mu \mathcal{R}(\omega_\mu, V) \right]^2 \simeq \hat{\sigma}^2 \frac{1}{N} \sum_{\mu=1}^{M} \mathcal{R}^2(\omega_\mu, V) \tag{218}$$

---

[12] AMP stands for *Approximate Message Passing*. This algorithm was first applied to compressed sensing in [100] and further developed in [101]. The way in which we have derived it closely follows [97].

[13] In order to do that there is an important point regarding the iteration procedure and the associated time indices that must be taken into account in order to have convergence. This was underlined in [102, 103] and we will not discuss this point but the interested reader can look at [97] for a review.

so that

$$\frac{q}{(1-q)^2} = \frac{1}{N}\sum_{\mu=1}^{M} \mathcal{R}^2(\omega_\mu, V) \tag{219}$$

Taking back the equation for $\omega_\mu$ we can easily see that $\omega_\mu$ converges in the large $N$ limit to a Gaussian variable with zero mean and variance $q$. Therefore

$$\frac{1}{N}\sum_{\mu=1}^{M} \mathcal{R}^2(\omega_\mu, V) \simeq \alpha \int_{-\infty}^{\infty} \frac{\mathrm{d}z}{\sqrt{2\pi q}} e^{-z^2/(2q)} \mathcal{R}^2(z, 1-q) \tag{220}$$

and therefore the equation for $q$ is given by

$$\frac{q}{(1-q)^2} = \alpha \int_{-\infty}^{\infty} \frac{\mathrm{d}z}{\sqrt{2\pi q}} e^{-z^2/(2q)} \mathcal{R}^2(z, 1-q)\,. \tag{221}$$

which is the replica symmetric saddle point equation. Therefore the TAP equations give the same result as the replica approach at the replica symmetric level. The way in which we got back the RS result is known as the State-Evolution analysis in computer science and machine learning [97].

## VI. CONCLUSIONS

In this lectures we have introduced two main techniques to study the properties of glassy systems namely the replica and cavity method. We have applied them to a model, the spherical random perceptron which is a toy model for both CSP and glasses. We have studied its phase diagram and the phase transitions where the model goes from a replica symmetric phase to regions where replica symmetry is broken. We have discussed the physical meaning of replica symmetry breaking and we have shown that the jamming transition lies in a so called marginal or fullRSB phase. Finally we have studied the critical behavior arising at jamming and we have shown how to compute the critical exponents. In the last part of these notes we have reviewed the TAP approach to this model and we have shown how it can be interpreted in an algorithmic way. Finally we have shown how the two approaches give the same results in the replica symmetric phase.



### Aknowledgments

I would like to thank Riccardo Guida and Sylvain Ribault for organizing the lectures and especially Riccardo for having taken care all the developments of these notes and their diffusion. Furthermore I would like thank the students and participants that attended the lectures and that helped me in improving the presentation. This work is supported by "Investissements d'Avenir" LabEx PALM (ANR-10-LABX-0039-PALM).

[1] D. Levine and P. J. Steinhardt, Physical review letters **53**, 2477 (1984).
[2] G. Parisi and F. Zamponi, Rev. Mod. Phys. **82**, 789 (2010).
[3] P. Charbonneau, J. Kurchan, G. Parisi, P. Urbani, and F. Zamponi, Annual Review of Condensed Matter Physics **8**, 265 (2017).
[4] W. Krauth, *Statistical Mechanics: Algorithms and Computations* (Oxford University Press, USA, 2006).
[5] M. S. Viazovska, Annals of Mathematics **185**, 991 (2017).

[6] H. Cohn, A. Kumar, S. D. Miller, D. Radchenko, and M. Viazovska, Annals of Mathematics **185**, 1017 (2017).

[7] J. H. Conway and N. J. A. Sloane, *Sphere Packings, Lattices and Groups* (Spriger-Verlag, New York, 1993).

[8] G. Parisi, Journal of Statistical Physics **132**, 207 (2008).

[9] G. Parisi and F. Zamponi, Journal of Statistical Mechanics: Theory and Experiment **2006**, P03017 (2006), URL `http://stacks.iop.org/1742-5468/2006/P03017`.

[10] T. Castellani and A. Cavagna, Journal of Statistical Mechanics: Theory and Experiment **2005**, P05012 (2005).

[11] G. Brambilla, D. El Masri, M. Pierno, L. Berthier, L. Cipelletti, G. Petekidis, and A. B. Schofield, Physical review letters **102**, 085703 (2009).

[12] A. Liu, S. Nagel, W. Van Saarloos, and M. Wyart, in *Dynamical Heterogeneities and Glasses*, edited by L. Berthier, G. Biroli, J.-P. Bouchaud, L. Cipelletti, and W. van Saarloos (Oxford University Press, 2011), `arXiv:1006.2365`.

[13] M. Wyart, Annales de Physique **30**, 1 (2005), `arXiv:cond-mat/0512155`, URL `http://www.citebase.org/abstract?id=oai:arXiv.org:cond-mat/0512155`.

[14] M. Wyart, Phys. Rev. Lett. **109**, 125502 (2012).

[15] M. Wyart, S. Nagel, and T. Witten, Europhysics Letters **72**, 486 (2005).

[16] M. Müller and M. Wyart (2015).

[17] G. Tarjus, in *Dynamical Heterogeneities and Glasses*, edited by L. Berthier, G. Biroli, J.-P. Bouchaud, L. Cipelletti, and W. van Saarloos (Oxford University Press, 2011), `arXiv:1010.2938`.

[18] L. Berthier and G. Biroli, Rev. Mod. Phys. **83**, 587 (2011), URL `http://link.aps.org/doi/10.1103/RevModPhys.83.587`.

[19] T. R. Kirkpatrick and P. G. Wolynes, Phys. Rev. A **35**, 3072 (1987).

[20] T. R. Kirkpatrick and P. G. Wolynes, Phys. Rev. B **36**, 8552 (1987).

[21] T. R. Kirkpatrick, D. Thirumalai, and P. G. Wolynes, Phys. Rev. A **40**, 1045 (1989).

[22] G. Biroli and J. Bouchaud, in *Structural Glasses and Supercooled Liquids: Theory, Experiment and Applications*, edited by P.G.Wolynes and V.Lubchenko (Wiley & Sons, 2012), `arXiv:0912.2542`.

[23] W. Kauzmann, Chem Rev **43**, 219 (1948).

[24] M. Mézard, G. Parisi, and M. A. Virasoro, *Spin glass theory and beyond* (World Scientific, Singapore, 1987).

[25] J. Kurchan, G. Parisi, and F. Zamponi, Journal of Statistical Mechanics: Theory and Experiment **2012**, P10012 (2012).

[26] J. Kurchan, G. Parisi, P. Urbani, and F. Zamponi, J. Phys. Chem. B **117**, 12979 (2013).

[27] P. Charbonneau, J. Kurchan, G. Parisi, P. Urbani, and F. Zamponi, Nature Communications **5**, 3725 (2014).

[28] P. Charbonneau, J. Kurchan, G. Parisi, P. Urbani, and F. Zamponi, J. Stat. Mech.: Theor. Exp. **2014**, P10009 (2014).

[29] C. Rainone, P. Urbani, H. Yoshino, and F. Zamponi, Phys. Rev. Lett. **114**, 015701 (2015).

[30] C. Rainone and P. Urbani, Journal of Statistical Mechanics: Theory and Experiment **2016**, 053302 (2016).

[31] T. Maimbourg, J. Kurchan, and F. Zamponi, Physical review letters **116**, 015902 (2016).

[32] W. Götze, *Complex dynamics of glass-forming liquids: A mode-coupling theory*, vol. 143 (OUP Oxford, 2008).

[33] R. Monasson, Phys. Rev. Lett. **75**, 2847 (1995).

[34] M. Mezard and A. Montanari, *Information, physics, and computation* (Oxford University Press, 2009).

[35] F. Zamponi, `arXiv:1008.4844` (2010).

[36] S. Arora and B. Barak, *Computational complexity: a modern approach* (Cambridge University Press, 2009).

[37] F. Krzakala, A. Montanari, F. Ricci-Tersenghi, G. Semerjian, and L. Zdeborova, Proceedings of the National Academy of Sciences **104**, 10318 (2007).

[38] M. Mézard and G. Parisi, The European Physical Journal B-Condensed Matter and Complex Systems **20**, 217 (2001).

[39] M. Mézard, G. Parisi, and R. Zecchina, Science **297**, 812 (2002).

[40] M. Mézard, F. Ricci-Tersenghi, and R. Zecchina, Journal of Statistical Physics **111**, 505 (2003).

[41] A. Braunstein, M. Mézard, and R. Zecchina, Random Structures & Algorithms **27**, 201 (2005).

[42] L. Zdeborová and F. Krzakala, Physical Review E **76**, 031131 (2007).

[43] R. J. Baxter, *Exactly solved models in statistical mechanics* (Elsevier, 2016).

[44] F. Krzakala and L. Zdeborová, EPL (Europhysics Letters) **81**, 57005 (2008).

[45] S. Franz and G. Parisi, arXiv:1501.03397 (2015).
[46] S. Franz, G. Parisi, M. Sevelev, P. Urbani, and F. Zamponi, arXiv preprint arXiv:1702.06919 (2017).
[47] F. Rosenblatt, Psychological review **65**, 386 (1958).
[48] E. Gardner, EPL (Europhysics Letters) **4**, 481 (1987).
[49] E. Gardner, Journal of physics A: Mathematical and general **21**, 257 (1988).
[50] E. Gardner and B. Derrida, Journal of Physics A: Mathematical and general **21**, 271 (1988).
[51] M. Mézard, Journal of Physics A: Mathematical and General **22**, 2181 (1989).
[52] V. Lubchenko and P. G. Wolynes, Annual Review of Physical Chemistry **58**, 235 (2007), arXiv.org:cond-mat/0607349.
[53] P. Wolynes and V. Lubchenko, eds., *Structural Glasses and Supercooled Liquids: Theory, Experiment, and Applications* (Wiley, 2012).
[54] W. Götze, *Complex dynamics of glass-forming liquids: A mode-coupling theory*, vol. 143 (Oxford University Press, USA, 2009).
[55] L. Berthier, G. Biroli, J.-P. Bouchaud, L. Cipelletti, and W. van Saarloos, eds., *Dynamical Heterogeneities and Glasses* (Oxford University Press, 2011).
[56] A. Cavagna, Physics Reports **476**, 51 (2009).
[57] G. Parisi, arXiv preprint cond-mat/0301157 (2003).
[58] M. Mezard and G. Parisi, in *Structural Glasses and Supercooled Liquids: Theory, Experiment and Applications*, edited by P.G.Wolynes and V.Lubchenko (Wiley & Sons, 2012), arXiv:0910.2838.
[59] T. R. Kirkpatrick and D. Thirumalai, Phys. Rev. B **36**, 5388 (1987).
[60] L. F. Cugliandolo and J. Kurchan, Phys. Rev. Lett. **71**, 173 (1993).
[61] J. Bouchaud, L. Cugliandolo, J. Kurchan, and M. Mezard, in *Spin glasses and random fields*, edited by A. Young (World Scientific, 1998), arXiv.org:cond-mat/9702070.
[62] S. Franz and G. Parisi, Journal de Physique I **5**, 1401 (1995).
[63] G. Biroli and P. Urbani, Nature Physics **12**, 1130 (2016).
[64] G. Biroli and P. Urbani, arXiv preprint arXiv:1704.04649 (2017).
[65] R. Monasson, R. Zecchina, S. Kirkpatrick, B. Selman, and L. Troyansky, nature **400**, 133 (1999).
[66] R. Monasson and R. Zecchina, Physical Review E **56**, 1357 (1997).
[67] F. Krzakala and J. Kurchan, Physical Review E **76**, 021122 (2007).
[68] D. J. Amit, *Modeling brain function: The world of attractor neural networks* (Cambridge University Press, 1992).
[69] V. Dotsenko, *An introduction to the theory of spin glasses and neural networks*, vol. 54 (World Scientific, 1995).
[70] J. A. Hertz, A. S. Krogh, and R. G. Palmer, *Introduction to the theory of neural computation*, vol. 1 (Basic Books, 1991).
[71] G. Györgyi, Physics Reports **342**, 263 (2001).
[72] G. Parisi, Physics Letters A **73**, 203 (1979).
[73] G. Parisi, Journal of Physics A: Mathematical and General **13**, L115 (1980).
[74] G. Parisi, Physical Review Letters **50**, 1946 (1983).
[75] H. Nishimori, *Statistical physics of spin glasses and information processing: an introduction*, vol. 111 (Clarendon Press, 2001).
[76] J. De Almeida and D. J. Thouless, Journal of Physics A: Mathematical and General **11**, 983 (1978).
[77] D. J. Thouless, J. R. L. de Almeida, and J. M. Kosterlitz, Journal of Physics C: Solid State Physics **13**, 3271 (1980).
[78] S. Kirkpatrick and D. Sherrington, Physical Review B **17**, 4384 (1978).
[79] A. Blandin, M. Gabay, and T. Garel, Journal of Physics C: Solid State Physics **13**, 403 (1980).
[80] M. Talagrand, *Spin glasses: a challenge for mathematicians: cavity and mean field models*, vol. 46 (Springer Science & Business Media, 2003).
[81] D. Panchenko, *The Sherrington-Kirkpatrick model* (Springer Science & Business Media, 2013).
[82] F. Guerra and F. L. Toninelli, Communications in Mathematical Physics **230**, 71 (2002).
[83] D. Panchenko, arXiv preprint arXiv:1112.1003 (2011).
[84] M. Mézard, G. Parisi, N. Sourlas, G. Toulouse, and M. Virasoro, Physical review letters **52**, 1156 (1984).

[85] R. Rammal, G. Toulouse, and M. A. Virasoro, Reviews of Modern Physics **58**, 765 (1986).
[86] M. Mézard and G. Parisi, Journal de Physique I **1**, 809 (1991).
[87] B. Duplantier, Journal of Physics A: Mathematical and General **14**, 283 (1981).
[88] H.-J. Sommers and W. Dupont, Journal of Physics C: Solid State Physics **17**, 5785 (1984).
[89] C. De Dominicis and I. Kondor, Physical Review B **27**, 606 (1983).
[90] I. Kondor and C. de Dominicis, EPL (Europhysics Letters) **2**, 617 (1986).
[91] A. Crisanti and C. De Dominicis, Philosophical Magazine **92**, 280 (2012).
[92] A. V. Goltsev, Journal of Physics A: Mathematical and General **16**, 1337 (1983).
[93] P. Anderson, Les Houches Session XXXI p. 161 (1979).
[94] P. Charbonneau, E. I. Corwin, G. Parisi, and F. Zamponi, Physical review letters **114**, 125504 (2015).
[95] M. Mézard, Physical Review E **95**, 022117 (2017).
[96] A. Altieri, S. Franz, and G. Parisi, Journal of Statistical Mechanics: Theory and Experiment **2016**, 093301 (2016).
[97] L. Zdeborová and F. Krzakala, Advances in Physics **65**, 453 (2016).
[98] A. Dembo, A. Montanari, et al., The Annals of Applied Probability **20**, 565 (2010).
[99] A. Dembo, A. Montanari, et al., Brazilian Journal of Probability and Statistics **24**, 137 (2010).
[100] D. L. Donoho, A. Maleki, and A. Montanari, Proceedings of the National Academy of Sciences **106**, 18914 (2009).
[101] F. Krzakala, M. Mézard, F. Sausset, Y. Sun, and L. Zdeborová, Physical Review X **2**, 021005 (2012).
[102] E. Bolthausen, Communications in Mathematical Physics **325**, 333 (2014).
[103] M. Bayati and A. Montanari, IEEE Transactions on Information Theory **57**, 764 (2011).
[104] L. F. Cugliandolo, in *Slow Relaxations and nonequilibrium dynamics in condensed matter* (Springer, 2003), pp. 367–521.
[105] E. Agoritsas, G. Biroli, P. Urbani, and F. Zamponi, arXiv preprint arXiv:1710.04894 (2017).
[106] S. Franz, G. Parisi, P. Urbani, and F. Zamponi, Proceedings of the National Academy of Sciences **112**, 14539 (2015).